

The Dominant Role of Critical Valence Fluctuations on High T_c Superconductivity in Heavy Fermions

Gernot W. Scheerer*

DQMP - University of Geneva, 1211 Geneva 4, Switzerland.

Zhi Ren

*Institute of Natural Sciences, Westlake Institute For Advanced Study,
Westlake University, 18 Shilongshan Road, Hangzhou 310024, P. R. China.*

Shinji Watanabe

*Department of Basic Sciences, Kyushu Institute of Technology,
Kitakyushu, Fukuoka, 804-8550, Japan.*

G rard Lapertot

PHELIQS, UMR-E 9001, CEA-INAC/UJF-Grenoble 1, 38054 Grenoble, France.

Dai Aoki

*Institute for Materials Research, Tohoku University,
Oarai, Ibaraki, 311-1313, Japan and
PHELIQS, UMR-E 9001, CEA-INAC/UJF-Grenoble 1, 38054 Grenoble, France.*

Didier Jaccard

DQMP - University of Geneva, 1211 Geneva 4, Switzerland.

Kazumasa Miyake

*Center for Advanced High Magnetic Field Science,
Osaka University, Toyonaka, Osaka, 560-0043, Japan.*

(Dated: September 6, 2018)

Abstract

Despite almost 40 years of research, the origin of heavy-fermion superconductivity is still strongly debated. Especially, the pressure-induced enhancement of superconductivity in CeCu_2Si_2 away from the magnetic breakdown is not sufficiently taken into consideration. As recently reported in CeCu_2Si_2 and several related compounds, optimal superconductivity occurs at the pressure of a valence crossover, which arises from a virtual critical end point at negative temperature T_{cr} . In this context, we did a meticulous analysis of a vast set of top-quality high-pressure electrical resistivity data of several Ce-based heavy fermion compounds. The key novelty is the salient correlation between the superconducting transition temperature T_{c} and the valence instability parameter T_{cr} , which is in line with theory of enhanced valence fluctuations. Moreover, it is found that, in the pressure region of superconductivity, electrical resistivity is governed by the valence crossover, which most often manifests in scaling behavior. We develop the new idea that the optimum superconducting T_{c} of a given sample is mainly controlled by the compound's T_{cr} and limited by non-magnetic disorder. In this regard, the present study provides compelling evidence for the crucial role of critical valence fluctuations in the formation of Cooper pairs in Ce-based heavy fermion superconductors besides the contribution of spin fluctuations near magnetic quantum critical points, and corroborates a plausible superconducting mechanism in strongly correlated electron systems in general.

* gernot.scheerer@unige.ch

I. INTRODUCTION

Superconductivity (SC) in heavy fermion (HF) systems is most often considered as being mediated by critical spin fluctuations [1–4]. Such a prevailing view is mainly derived from the presence of a magnetic instability regime leading to the collapse of long-range antiferromagnetic (AF) order at a critical p_c , concomitant with the emergence of SC. However in a few cases, SC has been ascribed to critical valence fluctuations (CVF) in the pressure region of the highest superconducting transition temperature T_c , in particular for CeCu_2Ge_2 [5, 6], CeCu_2Si_2 [7, 8], and CeRhIn_5 [9, 10]. The main ingredient of this interpretation is the existence in the pressure-temperature (p - T) plane of an underlying first-order valence transition, whose critical end point (CEP) occurs at pressure p_{cr} and at slightly negative temperature T_{cr} (see Fig. 1). With a negative T_{cr} , only a valence crossover (VCO) regime is accessible at finite temperature and the corresponding crossover line lies close to optimal SC. In the case of the prototype HF superconductor CeCu_2Si_2 , multiple experimental evidence of the VCO and CVF mediated SC has been reported in [5, 7, 8, 11–14]. For instance, direct, microscopic observation of the VCO and the absence of spin fluctuations close to optimal SC have been reported for CeCu_2Si_2 [13] and also CeIrIn_5 [15, 16] via Cu- and In-nuclear quadrupole resonance measurements, respectively.

Selected examples of p - T magnetic and superconducting phase diagrams of Ce-based HF superconductors are represented schematically in Fig. 1. The common feature of all compounds is that SC is optimal at a pressure close to p_{cr} . On the other hand, the magnetic p_c can coincide with p_{cr} as in the case of CeRhIn_5 [17], CePd_2Si_2 (this work), and CeAu_2Si_2 [18], or be much lower than p_{cr} as in CeCu_2Si_2 [8]. The spreading of SC over the pressure axis varies considerably and SC can even emerge deep inside the magnetic phase of CeAu_2Si_2 [18].

As a matter of interest, the CVF mechanism shares common aspects with the d-p charge transfer instability in high- T_c cuprates, which has been proposed to be at the origin of marginal Fermi liquid and non-Fermi liquid properties, and the pseudo-gap state [20, 21]. Moreover, valence fluctuations of Pu ions have been advocated as the source of “high- T_c ” in PuCoGa_5 [22]. Thus, we believe that the valence fluctuation physics discussed in this paper is pertinent for a larger community beyond that of HFs.

The microscopic-theoretical basis of the CVF scenario results from the inclusion of the

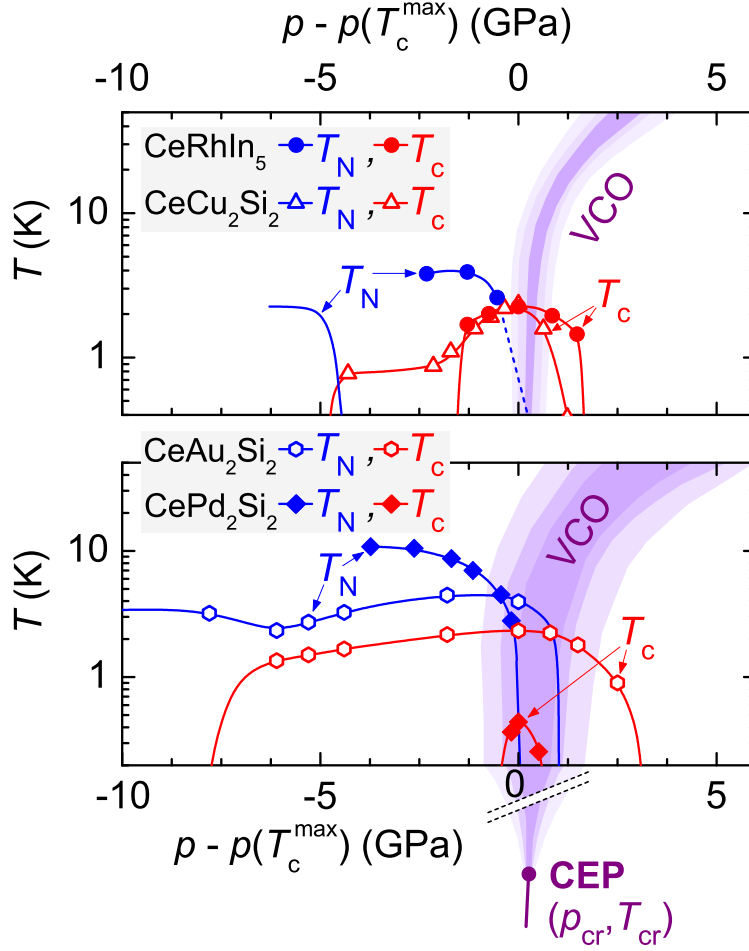


FIG. 1. **Examples of schematic p - T magnetic and superconducting phase diagrams of Ce-based HF superconductors.** Symbols stand for representative data points from CeRhIn₅ [17], CeCu₂Si₂ [8], CeAu₂Si₂ [18], and CePd₂Si₂ [19]: Néel temperature T_N and bulk-superconducting T_c . The graded-colored area represents the valence crossover.

additional term $H_{U_{fc}} = U_{fc} \sum_{i=1}^N n_i^f n_i^c$ in the periodic Anderson model, where U_{fc} is the Coulomb repulsion between f and conduction electrons [23, 24]. The physical origin of the T_c enhancement is the increase in the effective quasiparticle Fermi energy and the constancy of the dimensionless coupling for the Cooper pairing, following a BCS-like expression for T_c . The former factor stems from the valence crossover from the Kondo to the valence fluctuation region and the latter one is a result of the compensation between the decrease of the quasiparticle density of states and the increase in the pairing interaction, which is mediated by valence fluctuations associated with a sharp valence crossover.

Five years ago, thanks to an experimental progress [25] yielding more accurate electrical resistivity measurements on CeCu₂Si₂ under pressure up to 7 GPa, we have introduced a

method to estimate the temperature T_{cr} of the CEP [8]. Subsequently, the same process was successfully used for CeAu_2Si_2 [18, 26, 27]. In the present paper, this method is applied to all appropriate resistivity data established in Geneva since 1998, including new data notably from CeAg_2Si_2 , CeRhIn_5 and CeIrIn_5 . On the basis of 17 data sets from 9 different Ce-based HF compounds, the universal character of the relationship between the superconducting transition temperature T_c and the strength of the valence instability is unveiled. Taking into account the superconducting pair-breaking effect of non-magnetic disorder, quantified by the residual resistivity ρ_0 , we identify the two main parameters T_{cr} and ρ_0 controlling T_c of a representative part of Ce-based HF superconductors, which is consistent with the CVF theory. Moreover, it is found that, in the VCO regime of the p - T plane, electrical resistivity most often follows scaling behavior, underlining the role of valence fluctuation physics.

II. RESULTS

Figure 2 displays a 3D plot of the superconducting T_c as function of both the residual resistivity ρ_0 and the valence instability parameter T_{cr} based on published and new results (see Table S1 of the Supplementary Material for details and references). In this paper “ T_c ” refers to the maximum value of the bulk-superconducting transition temperature versus pressure for a given sample. Evidently in Fig. 2, all compounds except CeCu_5Au lie more or less on an empirically drawn inclined surface with a maximum for small ρ_0 and T_{cr} , which suggests that the superconducting T_c of a given sample is mainly controlled by the compound’s T_{cr} and the sample’s ρ_0 . T_c seems to culminate at ~ 2.5 K when $T_{\text{cr}} \rightarrow 0$ and $\rho_0 \rightarrow 0$, i.e., for a quantum CEP and negligible pair breaking effect. However, high ρ_0 values or large negative T_{cr} depress T_c .

We underline that all samples with $T_c > 2$ K are found to exhibit $-15 \text{ K} < T_{\text{cr}} < 0 \text{ K}$ and emphasize the striking relationship between the superconducting T_c , the parameter T_{cr} of the valence transition CEP, and pair breaking due to non-magnetic impurities (ρ_0). We introduce the expression “high- T_c ” to refer to the fact that the compounds with the highest T_c amongst the Ce-based HF superconductors are especially well represented in Fig. 2. Five out of the nine studied compounds have T_c higher than 1.5 K. At the moment, important cases like CeCoIn_5 [28], CeRh_2Si_2 [29], CePt_2In_7 [30], or non-centrosymmetric CePt_3Si [31] are lacking for different reasons (see below). Nevertheless, Fig. 2 represents a substantial

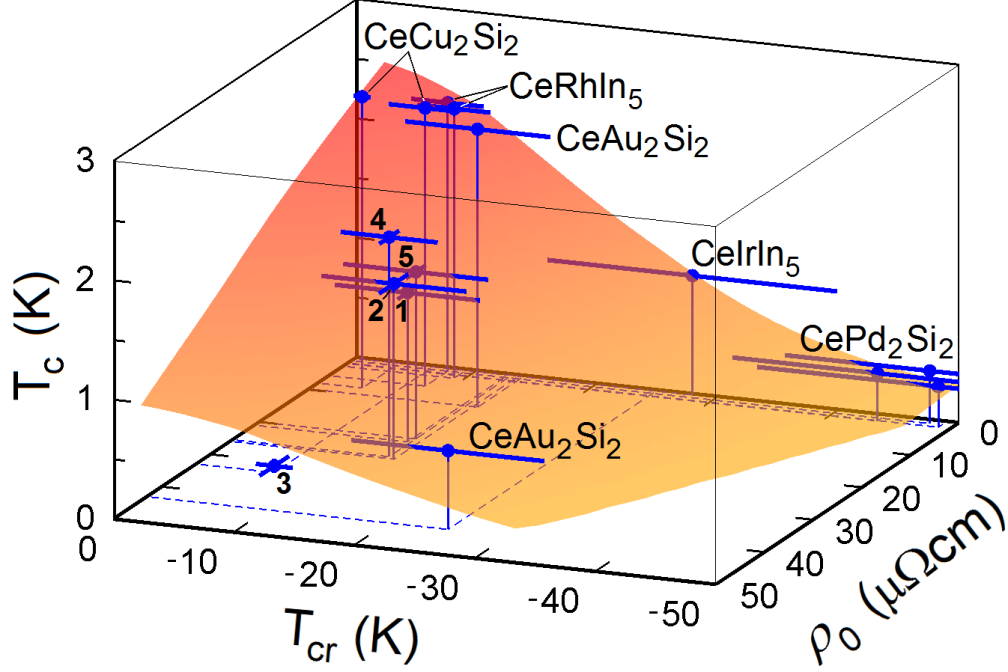


FIG. 2. Maximal superconducting T_c of Ce-based HF superconductors as a function of the key parameter T_{cr} and the residual resistivity ρ_0 . See text for details. Bold numbers indicate: $\text{CeAg}_2\text{Si}_2 = 1$, $\text{CeCu}_2\text{Ge}_2 = 2$, $\text{CeCu}_5\text{Au} = 3$, and other samples of $\text{CeCu}_2\text{Si}_2 = 4$ and $\text{CeAu}_2\text{Si}_2 = 5$. The error bars for T_{cr} represent estimated errors according the scaling analysis (see main text) and the error bars for ρ_0 result from the power-law extrapolation to zero temperature of $\rho(T)$. All compounds lie on or not far from the empirically drawn surface. Blue (violet) data points lie above (below) the surface. The surface is drawn for $T_{cr} \leq -2$ K for a reason discussed below and for $T_c \geq 0.28$ K, since no reliable information exists for very negative T_{cr} or very high ρ_0 .

part of Ce-based HF compounds and gives a unified view on their SC.

Before taking a closer look to the relationships $T_c(T_{cr})$ and $T_c(\rho_0)$, let us discuss the behavior of electrical resistivity ρ in the VCO regime and summarize the method for extracting T_{cr} from low-temperature ρ [8]. First, in Figure 3(a) we compare the schematic p - T phase diagrams of CeCu_2Si_2 and elementary Ce. In Ce, a first-order valence transition (FOVT) occurs at finite temperature due to small Ce-Ce ion spacing and therefore strong U_{fc} -repulsion between f- and conduction electrons at the same Ce site. The CEP lies at $p_{cr} \approx 1.5$ GPa and $T_{cr} \approx 480$ K [32]. As a function of pressure, isothermal resistivity of Ce [Fig. 3(b)] exhibits a discontinuous anomaly at the FOVT ($T < T_{cr}$) [33]. In the crossover regime ($T > T_{cr}$), isothermal resistivity decreases rapidly but continuously and the resistivity gradient diverges just at the CEP ($T \rightarrow T_{cr}$). In CeCu_2Si_2 , the CEP lies at slightly negative temperature $T_{cr} \approx -8$ K and, in the VCO regime, isothermal ρ decreases more

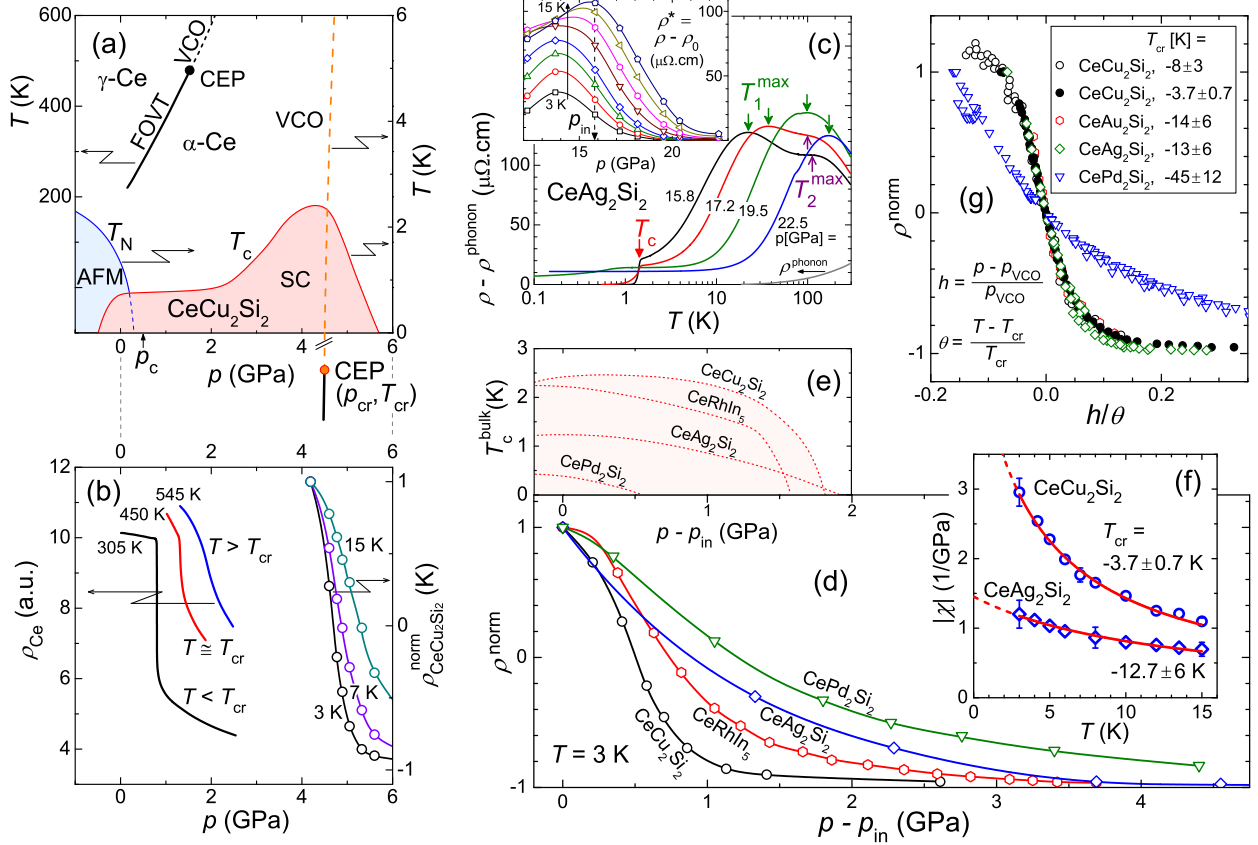


FIG. 3. **Extracting the negative temperature T_{cr} of the valence transition critical end point (CEP) from low- T resistivity.** (a) Schematic p - T phase diagrams of elementary Ce [32] and CeCu_2Si_2 [8]. (b) Isothermal resistivity ρ versus pressure p of Ce in vicinity of the valence transition CEP [33] and normalized resistivity ρ^{norm} vs p of CeCu_2Si_2 in the VCO regime. (c) Resistivity $\rho - \rho^{\text{phonon}}$ versus temperature T of CeAg_2Si_2 at selected pressures. Inset: Resistivity isotherms $\rho^* = \rho - \rho_0$ of CeAg_2Si_2 versus pressure at temperatures from 3 to 15 K. (d) ρ^{norm} versus $p - p_{\text{in}}$ of CeCu_2Si_2 , CeRhIn_5 , CeAg_2Si_2 , and CePd_2Si_2 at 3 K. The lines are guides to the eyes. (e) Schematic diagram of bulk SC for the same compounds (same p -scale as in (d)). (f) Slope $\chi = |d\rho^{\text{norm}}/dp|_{p_{\text{VCO}}}$ versus temperature T of CeCu_2Si_2 and CeAg_2Si_2 . The red lines represent fits to the data with $\chi \propto (T - T_{\text{cr}})^{-1}$. Error bars on χ , shown for representative data points, correspond to the over- and underestimation of χ due to a low p -run density. (g) Normalized resistivity ρ^{norm} versus the generalized distance h/θ from the CEP of CeCu_2Si_2 , CeAu_2Si_2 , CeAg_2Si_2 , and CePd_2Si_2 . (c-g) See Supplementary Table 1 for references.

and more rapidly versus pressure as temperature goes down without reaching a first-order discontinuity [8].

For a detailed analysis, the p -dependence of $\rho^* = \rho - \rho_0$ at several temperatures is derived from $\rho(T)$ of successive pressure runs, as shown for CeAg_2Si_2 in Fig. 3(c). A preliminary remark is that in all Ce-HF compounds the resistivity ρ^* is strongly reduced by 1 – 2 orders of magnitude, when the system is tuned by pressure through the VCO. Such a reduction,

which exceeds that expected for a progressive increase of the c-f hybridization, is attributed to a more or less sudden delocalization of 4f electrons [12]. In order to disentangle the intrinsic effect of electron delocalization from that of the temperature-dependent scattering rate, the resistivity has to be normalized. For this purpose we define an initial pressure p_{in} , which signals the onset of the VCO resistivity collapse (see inset of Fig. 3(c) and page 9 of the Supplementary Material for CePd₂Si₂). Then, the normalized resistivity $\rho^{\text{norm}} = \frac{\rho^*(p) - \rho^*(p_{\text{VCO}})}{\rho^*(p_{\text{VCO}})}$, where p_{VCO} is the pressure of the mid drop of ρ^* , is calculated for each temperature.

By way of example, Fig. 3(d) shows ρ^{norm} versus $p - p_{\text{in}}$ at 3 K of CeCu₂Si₂, CeRhIn₅, CeAg₂Si₂, and CePd₂Si₂. Clearly, it appears that the collapse of ρ^{norm} is always close to optimal SC and a steeper collapse favors higher T_c [see Fig. 3(e)]. With increasing temperature, i.e., increasing distance from the CEP, the pressure scale of the resistivity reduction gets broader and broader and the steepness of the collapse decreases, as shown for CeCu₂Si₂ in Fig. 3(b). Fig. 3(f) displays the temperature dependence of the slope $\chi = |d\rho^{\text{norm}}/dp|_{p_{\text{VCO}}}$ of CeCu₂Si₂ and CeAg₂Si₂. χ , which we interpret as valence susceptibility, tends to diverge as $\chi \propto (T - T_{\text{cr}})^{-1}$, i.e., a first-order discontinuity would occur in $\rho^*(p)$ for $T < T_{\text{cr}}$. Evidently, a simple fit to $\chi(T)$ yields T_{cr} . The empirical law $(T - T_{\text{cr}})^{-1}$ is confirmed by data from several samples of CeCu₂Si₂ [8], CeAu₂Si₂ [18, 26, 27], and CeRhIn₅ [17], which are by the way the compounds with highest T_c and least negative T_{cr} . Note that the plot of $\chi(T)$ is limited to a temperature (15 K), which corresponds to a small fraction of the first crystal-field-splitting energy. Such a treatment is repeated on all appropriate data from Ce-based HF compounds (see Supplementary Figs. S4–S13). The extracted T_{cr} values and other parameters (T_c , ρ_0) are summarized in Table S1 of the Supplementary Material.

After identifying T_{cr} , one can apply the scaling treatment developed in Ref. [8] for CeCu₂Si₂ within the framework of universal scaling theory of critical phenomena and subsequently applied on data from CeAu₂Si₂ [18, 26, 27] and CeRhIn₅ [17]. To this end, a generalized distance h/θ from the CEP is calculated, where $h = (p - p_{\text{VCO}})/p_{\text{VCO}}$ and $\theta = (T - T_{\text{cr}})/|T_{\text{cr}}|$. Then, for a given compound, all ρ^{norm} isotherms in the VCO regime collapse on a single curve $\rho^{\text{norm}} = f(h/\theta)$ when plotted versus h/θ , as shown in Fig. 3(g). This means that for the generalized distance h/θ from the CEP, the ρ^{norm} isotherms behave in a unique manner, which strongly supports the existence of the valence CEP at $(p_{\text{cr}}, T_{\text{cr}})$. Note that in terms of universal scaling theory of critical phenomena the equation is $\rho^{\text{norm}}/h^{1/\delta} = f(h/\theta^{\gamma\delta/(\delta-1)})$, with the critical exponents γ and δ (mean-field approach:

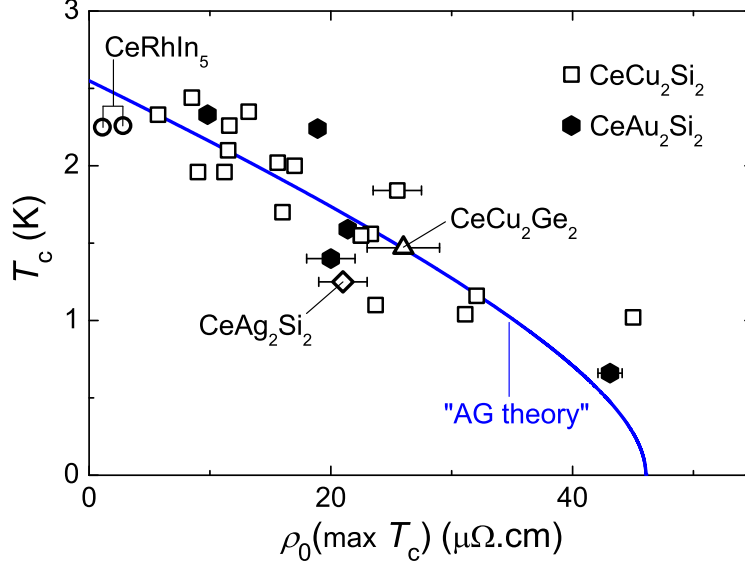


FIG. 4. **Pair-breaking systematics:** T_c vs ρ_0 (ρ_0 taken at the pressure of maximal T_c) of the CeCu_2Si_2 family and CeRhIn_5 (published and unpublished data, see Supplementary Fig. S1 for references). The error bars on ρ_0 result from the power-law extrapolation to zero temperature of $\rho(T)$. The solid line represents the generalized Abrikosov-Gor'kov theory with a critical resistivity $\rho_0^{\text{cr}} = 46 \mu\Omega\text{cm}$ [38].

$\gamma_{\text{MF}} = 1$, $\delta_{\text{MF}} = 3$). Accordingly to Ref. [8], the critical exponents are fixed as $\gamma = 1$ and $\delta \rightarrow \infty$, which does not correspond to a simple universality class.

The scaling is very robust for 15 data sets from 7 different systems and astonishingly the scaling function $f(h/\theta)$ is identical for the isovalent systems CeCu_2Si_2 , CeAg_2Si_2 , and CeAu_2Si_2 [see Fig. 3(g)]. However, $f(h/\theta)$ is different for CePd_2Si_2 and apparently material dependent. For instance $f(h/\theta)$ of CeCu_5Au (Supplementary Fig. S12) lies in between the two data sets of Fig. 3(g). The scaling fails for two data sets: the ρ^{norm} isotherms of CeCu_6 (Supplementary Fig. S11) and CeIrIn_5 (Supplementary Fig. S13) do not collapse on a single curve. Measurement errors surely play a role for the CeCu_6 sample (see Supplementary Fig. S11) and a change of regime ascribed to the crystal field effect [34] may interfere. In CeIrIn_5 , low-temperature resistivity properties hint to a pressure-induced change of regime (see Supplementary Fig. S13), which may explain that the isotherms collapse only for $h/\theta > 0$. Though, completely satisfactory explanations are still missing for both.

We now discuss the pair-breaking effect by disorder, which is quantified by the residual resistivity ρ_0 . Figure 4 shows T_c versus ρ_0 of the CeCu_2Si_2 family and CeRhIn_5 from all 26 independent pressure experiments done in Geneva with $\rho_0 < 50 \mu\Omega\text{cm}$ (see Supplementary

Fig. S1 for details and references). Not included are still finite T_c values corresponding to very high ρ_0 , which deviate from the general trend possibly due to alloying or Kondo-hole effects. For instance, in a $\text{CeCu}_2(\text{Si}_{1-x}\text{Ge}_x)_2$ alloy, a maximum bulk $T_c \sim 0.6$ K ($\rho = 0$ criteria) is reported for $\rho_0 \sim 70 \mu\Omega\text{cm}$ [35], and, in polycrystalline CeCu_2Si_2 , a maximum bulk $T_c \sim 0.3$ K is given with $\rho_0 \sim 180 \mu\Omega\text{cm}$, which is higher than the room temperature resistivity [36]. The evident decrease of T_c with increasing disorder follows qualitatively well the formula given by the Abrikosov-Gor'kov (AG) theory [37] generalized for non-magnetic disorder in a CVF-mediated d-wave superconductor with a critical resistivity $\rho_0^{\text{cr}} = 46 \mu\Omega\text{cm}$ [38]. Note that every data point in Fig. 4 refers to a set of pressure runs for an experiment on a sample of specific quality as reflected by its $\rho_0(p=0)$ value. Thus in spite of a given data scattering, the systematic dependence of T_c on ρ_0 for different samples of different compounds is remarkable.

A similar trend is observed for the $\text{CePd}_2(\text{Si/Ge})_2$ family, where bulk SC vanishes completely for ρ_0 higher than $3 \mu\Omega\text{cm}$ (see Supplementary Fig. S2). T_c is already small at ideal sample quality since these compounds are located far from the criticality as signaled by the large negative $T_{\text{cr}} \sim -50$ K. Therefore, the theory of Okada *et al.* [38] for robustness of T_c versus pair-breaking effect by non-magnetic disorder is not appropriate, and the conventional AG-theory for anisotropic superconductivity can be applied. The latter is valid for the d-wave order parameter predicted by the CVF theory [23] and accounts for the rapid decrease of T_c in CePd_2Si_2 .

The critical resistivity $\rho_0^{\text{cr}} \approx 46 \mu\Omega\text{cm}$ of the “high- T_c ” HF superconductors is far larger than that expected in the conventional case of weak-coupling SC but is compatible with the generalized AG theory [38]. In fact, due to the valence fluctuation renormalization effect of the impurity potential [39], ρ_0 is strongly increased at pressures around p_{cr} compared to far lower or higher pressures, which is a hallmark of CVF-mediated HF superconductors (exceptions are CeCu_6 [34] and CePd_2Si_2 [19]). The robustness of T_c against impurity scattering is due to the fact that the re-normalized impurity potential is a long-range like bare Coulomb potential [38, 39]. Indeed, almost all scattering channels with angular momentum $\ell = 0, 1, 2, \dots$, i.e., s-, p-, d-wave and so on, are active in the Coulomb-type potential, leading to partial cancellation in the scattering rate among the ℓ -wave vertex part in the pair susceptibility and the self-energy part in the Green function. This rationalizes the robustness of T_c against the enhanced impurity potential in contrast to the conventional

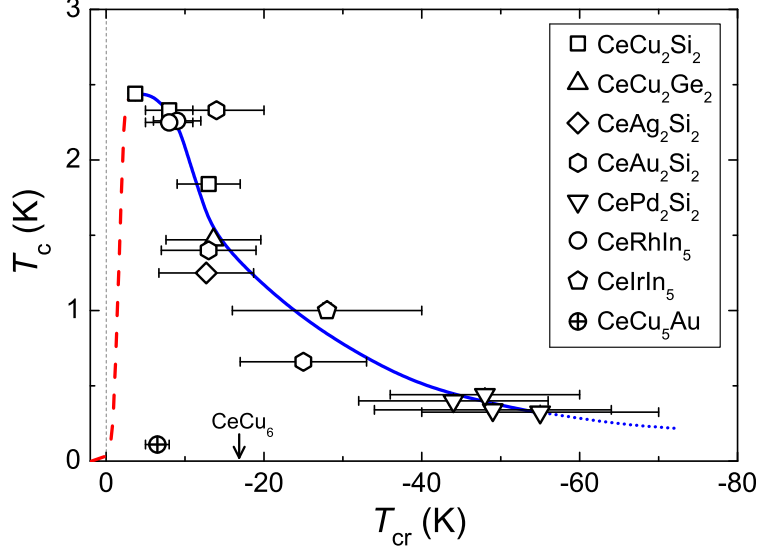


FIG. 5. **Building superconductivity up in heavy fermion compounds.** The presented T_c -vs- T_{cr} relation is qualitatively predicted by CVF theory [23, 24]. The continuous line is a guide to the eyes. The dashed line represents a qualitative prediction from CVF theory [23]. The error bars on T_{cr} represent estimated errors according the scaling analysis (see main text). The arrow indicates T_{cr} of CeCu_6 (no SC).

AG-type theory for anisotropic pairing, where essentially an s-wave component of impurity potential is taken into account [40, 41].

Figure 5 presents the most interesting relationship between T_c and the key parameter T_{cr} . T_c is maximal for small negative T_{cr} and decreases as T_{cr} becomes more negative, which is qualitatively predicted by CVF theory [23, 24]. About half of the data correspond to samples with almost optimal T_c for the specific compounds thanks to low ρ_0 values (see Supplementary Table S1), which underlines the intrinsic character of the T_c -vs- T_{cr} relationship. Unlike Fig. 4, less data points are presented because of the stringent requirement of accuracy and reliability of resistivity measurement for the scaling analysis, which excludes a part of our results and also those found in literature. In respect of the procedure to deduce T_{cr} , a prerequisite is the accurate control of the absolute resistivity value as function of pressure (form factor) and temperature and a high pressure run density. The control of the form factor is far to be an easy task in high-pressure cells and main complication comes from non-hydrostatic conditions in various pressure transmitting medium such as He [42, 43], Daphne oil [8, 25], or steatite [18, 44]. Another requirement is the limitation of non-systematic error on pressure and the precise estimation of ρ_0 . Moreover, due to the presumed $1/(T - T_{cr})$ dependence of χ , the uncertainty on T_{cr} is magnified for large negative

values, while the smallest values are the most accurate. Namely, in the case of CeCu_2Si_2 with $T_{\text{cr}} = -3.7$ K, the error is within the symbol size.

Despite reliable small T_{cr} and moderate ρ_0 , CeCu_6 (no SC) and CeCu_5Au (partial SC at 0.11 K) clearly lie below the general trend. From a literature review, small T_{cr} values should also be expected for some compounds including CeAl_2 [45], CeAl_3 [46, 47], and CeInCu_2 [48]. However, SC has never been observed in these cases. We have no satisfactory explanation yet for this discrepancy.

The dashed red curve for $T_{\text{cr}} \rightarrow 0$ in Fig. 5 is drawn from the theoretical prediction of the 3D model [23] in which T_c is paradoxically suppressed just at the critical point of the valence transition, while T_c takes sharp maximum near the VCO line in the Kondo regime. This aspect has also been verified by the density-matrix-renormalization-group calculation for the 1D model [24], which is numerically accurate. Namely, inter-site pairing correlation dominates over spin density wave and charge density wave correlations near the sharp VCO inside the Kondo regime.

III. DISCUSSION

The systematic behavior of T_c versus ρ_0 and T_{cr} points to a possible maximum $T_c \approx 2.5$ K in Ce-based HF superconductors and strongly supports that CVF provide the dominant pairing mechanism. Although, the relation between T_c and T_{cr} was already inferred in the pioneer work of Onishi and Miyake [23], a quantitative prediction seems almost impossible at the present state of art. Theory also considers that T_{cr} is influenced by disorder in general, which is less evident in the experimental data (see Supplementary Fig. S3). Naively, one can imagine that disorder induces an additional smearing of the VCO, which depresses T_{cr} and then T_c .

Let us now comment some generalities about magnetism and superconductivity in HF compounds. A hallmark is the merging close to p_{cr} of the two maxima in $\rho(T)$ [see Fig. 3(c)], which indicates that the rapidly rising Kondo energy starts to exceed the first crystal-field-splitting energy [49]. For HF superconductors, this pressure corresponds to optimal SC without exception. Crossing the VCO, the ground state degeneracy of the Ce ion increases from $n = 2$ to full degeneracy $n = 6$ of the 4f multiplet [7], and at the pressure of maximal T_c , the energy scale T_K is much larger than the magnetic ordering temperature. Moreover,

the strength of the f-c hybridization seems to control the position of p_c in respect to p_{cr} as shown theoretically [10]. In the case of strong hybridization p_c and p_{cr} are well separated, but in the case of weak hybridization a hypothetical magnetic QCP would occur at pressure higher than p_{cr} and the VCO drives a first-order collapse of magnetism at $p_c \sim p_{cr}$ [10, 50] in parallel to the traditional competition between the RKKY and Kondo energies. Hence the collapse of magnetism is very abrupt or even first-order-like in CeAu₂Si₂ [18, 51], CeAg₂Si₂ [52], and CeRhIn₅ [53].

Although pressure is a clean tuning parameter, clear evidence of a second-order magnetic transition down to zero temperature and a resulting quantum critical point is not well established from pressure investigations on pure lattices. In the particular case of CePd₂Si₂, results of Refs. [3, 43, 54, 55] support a linear decrease of T_N down to zero with p approaching p_c . However, a more rapid vanishing of T_N appears to correspond to higher superconducting T_c [19, 56] (see Supplementary Fig. S14). The difficulty of tracking the T_N vanishing with resistivity or even heat capacity probes and the unavoidable pressure gradient, due to which the T_N decrease appears more progressive, impedes a clear-cut conclusion. Seemingly second-order-like magnetic collapses have only been established for alloy systems, see e.g. [35, 57] and a lattice [58] with relatively high ρ_0 value, where disorder likely masks the intrinsic behavior.

The overlap of magnetic order and SC in CeRhIn₅ [50, 53] and especially in CeAu₂Si₂ [18] (see Fig. 1) contradicts the longstanding consensus that HF SC emerges in the vicinity of the magnetic border [4]. From a global point of view, the CeCu₂Si₂ family shows quite different magnetic phase diagrams concomitantly with otherwise strikingly similar electric and thermoelectric transport and superconducting properties [18, 27, 51]. For instance, a systematic feature in thermopower precedes the occurrence of SC [27]. Consequently, the link between SC and magnetism is primarily a competition, with the possible exception of CeAu₂Si₂ [18]. Up to a given delocalization of 4f electrons, magnetism hinders CVF to build up SC. On the other hand, the low-pressure SC pocket in CeCu₂Si₂ is the best candidate for spin fluctuation mediated SC [59], because the magnetic collapse at $p_c \approx 0$ and the VCO at $p_{cr} \approx 4.2$ GPa are exceptionally well separated. Though, the scenario of single-band nodal-d-wave SC at $p = 0$ in CeCu₂Si₂ is now strongly challenged [60–63].

Let us comment on the Kondo-volume-collapse mechanism introduced by Razafimandimby *et al.* [64]. To our understanding, it is essentially a phonon-mediated SC mechanism due

to enhanced electron-phonon coupling through the Kondo-volume-collapse effect (large Gruneisen parameter). In this regard, it should be different from the valence fluctuation mediated mechanism. According to an almost exact (justified by the Ward identity argument) theoretical discussion based on periodic Anderson model with coupling to phonon by Jichu *et al.* [65], it seems rather difficult for this mechanism to build up "high- T_c " SC in Ce-based heavy fermions. According to Jichu *et al.*, the enhanced pairing interaction (by Kondo-volume-collapse effect) vanishes at the static limit. Furthermore, it is crucial to note that the valence fluctuation mechanism is not based on density fluctuations but fluctuations of f-c charge transfer with the total charge density ($n_f + n_c$) essentially kept constant. Namely, valence fluctuations are rather categorized with orbital fluctuations.

Finally, we comment on CVF in Yb-based HF compounds, which can be approached as electron-hole/inverse-pressure analogues of Ce compounds. Interestingly, the first discovered Yb-based superconductor β -YbAlB₄ [66] exhibits normal state properties with unconventional quantum criticality [67], which is naturally explained by the CVF theory [68]. Furthermore, common criticality has been observed in some classes of Yb-based periodic crystals and even in the quasicrystal Yb₁₅Au₅₁Al₃₄ [69]. Search for superconductivity induced by CVF in Yb-based systems as well as the identification of the CEP of the underlying Yb-valence transition on the basis of the method described in this paper is expected to open a new frontier in this field.

For a long time, the spin-fluctuation-mediated mechanism was the mainstream scenario for SC in HF systems. However, the CVF theory has provided a new framework able to account for the high-pressure superconducting phase and several other phenomena in CeCu₂Si₂. We now have shown that this theory is able to explain salient experimental features in a multitude of systems, corroborating CVF as a plausible Cooper pairing mechanism. Concretely, the present study provides striking evidence that the optimum superconducting T_c in many Ce-based HF superconductors is essentially controlled by the strength of CVF and by non-magnetic disorder. Furthermore, we believe that CVF-induced SC is connected to a much wider part of non-trivial physics in strongly correlated electron systems including high- T_c cuprates [21, 70, 71]. Thus, our work uncovers a new playground for condensed matter physicists.

METHODS

The above presented results are based on electrical resistivity data obtained on 17 single crystals from 9 different Ce-based HF compounds (see Supplementary Table S1). The four-point electrical resistivity measurements under high-pressure conditions have been carried out in standard helium and dilution cryostats. The high-pressure conditions were obtained using Bridgman pressure cells with tungsten-carbide or diamond anvils and with different pressure transmitting medium. Technical details can be found for each transmitting medium in (helium) [7, 42], (Daphne oil) [8, 25], and (steatite) [18, 44]. All relevant information about crystals growth, dimension of sample and pressure cell, and data acquisition can be found in the respective references (see Supplementary Table S1). All relevant information about data treatment can be found in Ref. [8] and in the main text.

SUPPLEMENTARY MATERIAL

The Supplementary Material follows after the bibliography:

- Table S1
- Figures S1 to S14

ACKNOWLEDGMENTS

We acknowledge H. Wilhelm, S. Raymond, and A. T. Holmes for enabling the analysis of previous data, and M. Lopez, S. Müller, and M. Tran for technical support. D. Aoki acknowledges for the financial support KAKENHI (15H05882, 15H05884, 15K21732, 16H04006). K. Miyake acknowledges for the financial support KAKENHI (17K05555). S. Watanabe acknowledges for the financial support KAKENHI (15K05177, 16H01077).

AUTHOR CONTRIBUTIONS

D. J. conceived the idea and designed the experiment. D. A. and G. L. have grown the single crystal samples. G. S. and Z. R. performed the measurements. G. S. analyzed the

data. S. W. and K. M. provided the microscopic-theoretical interpretation. G. S. and D. J. wrote the paper. All authors discussed the results and commented on the manuscript.

-
- [1] K. Miyake, S. Schmitt-Rink, and C. M. Varma. Spin-fluctuation-mediated even-parity pairing in heavy-fermion superconductors *Phys. Rev. B* **34**, 6554-6556 (1986).
 - [2] D. J. Scalapino, E. Loh, Jr., and J. E. Hirsch. *d*-wave pairing near a spin-density-wave instability. *Phys. Rev. B* **34**, 8190-8192 (1986).
 - [3] N. D. Mathur *et al.* Magnetically mediated superconductivity in heavy fermion compounds. *Nature* **394**, 39-43 (1998).
 - [4] P. Monthoux, D. Pines, and G. G. Lonzarich. Superconductivity without phonons. *Nature* **450**, 1177-1183 (2007).
 - [5] D. Jaccard, H. Wilhelm, K. Alami-Yadri, and E. Vargoz. Magnetism and superconductivity in heavy fermion compounds at high pressure. *Physica B* **259-261**, 1-7 (1999).
 - [6] K. Miyake, O. Narikiyo, and Y. Onishi. Superconductivity of Ce-based heavy fermions under pressure: Valence fluctuation mediated pairing associated with valence instability of Ce. *Physica B* **259-261**, 676-677 (1999).
 - [7] A. T. Holmes, D. Jaccard, and K. Miyake. Signatures of valence fluctuations in CeCu₂Si₂ under high pressure. *Phys. Rev. B* **69**, 024508 (2004).
 - [8] G. Seyfarth *et al.* Heavy fermion superconductor CeCu₂Si₂ under high pressure: Multiprobing the valence crossover. *Phys. Rev. B* **85**, 205105 (2012).
 - [9] K. Miyake. New trend of superconductivity in strongly correlated electron systems. *J. Phys.: Condens. Matter* **19**, 125201 (2007).
 - [10] S. Watanabe and K. Miyake. Roles of critical valence fluctuations in Ce- and Yb-based heavy fermion metals. *J. Phys.: Condens. Matter* **23**, 094217 (2011).
 - [11] A. Holmes, D. Jaccard, and K. Miyake. Valence Instability and Superconductivity in Heavy Fermion Systems. *J. Phys. Soc. Jpn.* **76**, 051002 (2007) and Refs. [8,9,42,45,50,52,53] therein.
 - [12] J.-P. Rueff *et al.* Pressure-Induced Valence Crossover in Superconducting CeCu₂Si₂. *Phys. Rev. Lett.* **106**, 186405 (2011).
 - [13] K. Fujiwara *et al.* High Pressure NQR Measurement in CeCu₂Si₂ up to Sudden Disappearance of Superconductivity. *J. Phys. Soc. Jpn.* **77**, 123711 (2008).

- [14] T. C. Kobayashi *et al.* Valence Crossover of Ce Ions in CeCu₂Si₂ under High Pressure – Pressure Dependence of the Unit Cell Volume and the NQR Frequency–. *J. Phys. Soc. Jpn.* **82**, 114701 (2013).
- [15] S. Kawasaki *et al.* Enhancing the Superconducting Transition Temperature of the Heavy Fermion Compound CeIrIn₅ in the Absence of Spin Correlations. *Phys. Rev. Lett.* **94**, 037007 (2005).
- [16] M. Yashima *et al.* Possibility of Valence-Fluctuation-Mediated Superconductivity in Cd-Doped CeIrIn₅ Probed by In NQR. *Phys. Rev. Lett.* **109**, 117001 (2012).
- [17] Z. Ren *et al.* Coincidence of magnetic and valence quantum critical points in CeRhIn₅ under pressure. *Phys. Rev. B* **96**, 184524 (2017).
- [18] Z. Ren *et al.* Giant Overlap between the Magnetic and Superconducting Phases of CeAu₂Si₂ under Pressure. *Phys. Rev. X* **4**, 031055 (2014).
- [19] A. Demuer, A.T. Holmes, and D. Jaccard. Strain enhancement of superconductivity in CePd₂Si₂ under pressure. *J. Phys.: Condens. Matter* **14**, L529-L535 (2002).
- [20] C. M. Varma. Non-Fermi-liquid states and pairing instability of a general model of copper oxide metals. *Phys. Rev. B* **55**, 14554-14580 (1997).
- [21] C. M. Varma. Theory of the pseudogap state of the cuprates. *Phys. Rev. B* **73**, 155113 (2006).
- [22] B. J. Ramshaw *et al.* Avoided valence transition in a plutonium superconductor. *PNAS* **112**, 3285-3289 (2015).
- [23] Y. Onishi and K. Miyake. Enhanced Valence Fluctuations Caused by f-c Coulomb Interaction in Ce-Based Heavy Electrons: Possible Origin of Pressure-Induced Enhancement of Superconducting Transition Temperature in CeCu₂Ge₂ and Related Compounds. *J. Phys. Soc. Jpn.* **69**, 3955-3964 (2000).
- [24] S. Watanabe, M. Imada, and K. Miyake. Superconductivity Emerging near Quantum Critical Point of Valence Transition. *J. Phys. Soc. Jpn.* **75**, 043710 (2006).
- [25] A.-S. Ruetschi and D. Jaccard. Adaptation of the Bridgman anvil cell to liquid pressure mediums. *Rev. Sci. Instrum.* **78**, 123901 (2007).
- [26] Z. Ren, G. Girit, G. W. Scheerer, G. Lapertot, and D. Jaccard. Effect of disorder on the pressure-induced superconducting state of CeAu₂Si₂. *Phys. Rev. B* **91**, 094515 (2015).
- [27] Z. Ren, G. W. Scheerer, G. Lapertot, and D. Jaccard. Scaling behavior of temperature-dependent thermopower in CeAu₂Si₂ under pressure. *Phys. Rev. B* **94**, 024522 (2016).

- [28] C. Petrovic *et al.* Heavy-fermion superconductivity in CeCoIn₅ at 2.3 K. *J. Phys.: Condens. Matter* **13**, L337-L342 (2001).
- [29] S. Araki, M. Nakashima, R. Settai, T. C. Kobayashi, and Y. Ōnuki. Pressure-induced superconductivity in an antiferromagnet CeRh₂Si₂. *J. Phys.: Condens. Matter* **14**, L377-L383 (2002).
- [30] V. A. Sidorov *et al.* Pressure phase diagram and quantum criticality of CePt₂In₇ single crystals. *Phys Rev. B* **88**, 020503(R) (2013).
- [31] M. Nicklas *et al.* Pair breaking by nonmagnetic impurities in the noncentrosymmetric superconductor CePt₃Si. *Phys. Rev. B* **81**, 180511 (2010).
- [32] M. J. Lipp *et al.* Thermal Signatures of the Kondo Volume Collapse in Cerium. *Phys. Rev. Lett.* **101**, 165703 (2008).
- [33] A. Jayaraman. Fusion Curve of Cerium to 70 Kilobar and Phenomena Associated with Supercritical Behavior of fcc Cerium. *Phys. Rev.* **137**, A 179-182 (1965).
- [34] S. Raymond, D. Jaccard. High Pressure Resistivity of the Heavy Fermion Compound CeCu₆. *J. Low Temp. Phys.* **120**, 107-119 (2000).
- [35] H. Q. Yuan *et al.* Observation of Two Distinct Superconducting Phases in CeCu₂Si₂. *Science* **302**, 2104-2107 (2003).
- [36] A. T. Holmes, D. Jaccard, H. S. Jeevan, C. Geibel, M. Ishikawa. Anisotropy, disorder, and superconductivity in CeCu₂Si₂ under high pressure. *J. Phys.: Condens. Matter* **17**, 5423-5432 (2005).
- [37] A. A. Abrikosov and L. P. Gorkov, Zh. Eksp. Teor. Fiz. **39**, 1781 (1960) [Sov. Phys. JETP **12**, 1243 (1961)].
- [38] A. Okada and K. Miyake. Impurity Effect on Superconductivity in Critical-Valence-Fluctuations Region. *J. Phys. Soc. Jpn.* **80**, 084708 (2011).
- [39] K. Miyake and H. Maebashi. Huge Enhancement of Impurity Scattering due to Critical Valence Fluctuations in a Ce-Based Heavy Electron System. *J. Phys. Soc. Jpn.* **71**, 1007-1010 (2002).
- [40] S. Schmitt-Rink, K. Miyake, and C. M. Varma. Transport and Thermal Properties of Heavy-Fermion Superconductors: A Unified Picture. *Phys. Rev. Lett.* **57**, 2575-2578 (1986).
- [41] P. Hirschfeld, D. Vollhardt, and P. Wölfle. Resonant impurity scattering in heavy fermion superconductors. *Solid State Commun.* **59**, 111-115 (1986).

- [42] A. Holmes. Exotic superconducting mechanisms in Fe and CeCu_2Si_2 under pressure. *PhD thesis*, Université de Genève, Geneva (2004).
- [43] A. Demuer *et al.* Further pressure studies around the magnetic instability of CePd_2Si_2 . *J. Phys.: Condens. Matter* **13**, 9335-9347 (2001).
- [44] E. Vargoz, D. Jaccard, J.-Y. Genoud, J.-P. Brison, J. Flouquet. Upper critical field of CeCu_2Si_2 at very high pressure. *Solid State Commun.* **106**, 631-636 (1998).
- [45] H. Miyagawa *et al.* Electronic states of single crystal CeAl_2 near the pressure-induced quantum critical point. *Phys. Rev. B* **78**, 064403 (2008).
- [46] D. Jaccard and J. Sierro. Magnetic instability and superconductivity in cerium based HF compounds. *Physica B* **206** & **207**, 625-627 (1995).
- [47] G. Oomi and T. Kagayama. Effect of Pressure on the Magnetoresistance of the Heavy Fermion Compound CeAl_3 . *J. Phys. Soc. Jpn.* **65**, 2732-2733 (1996).
- [48] T. Kagayama, G. Oomi, H. Takahashi, N. Mōri, Y. Ōnuki, and T. Komatsubara. Pressure-induced valence instability of the heavy-fermion compound CeInCu_2 . *Phys. Rev. B* **44**, 7690-7693 (1991).
- [49] Y. Nishida, A. Tsuruta, and K. Miyake. Crystalline-Electric-Field Effect on the Resistivity of Ce-based Heavy Fermion Systems. *J. Phys. Soc. Jpn.* **75**, 064706 (2006).
- [50] S. Watanabe and K. Miyake. Origin of Drastic Change of Fermi Surface and Transport Anomalies in CeRhIn_5 under Pressure. *J. Phys. Soc. Jpn.* **79**, 033707 (2010).
- [51] G. W. Scheerer, G. Girit, Z. Ren, G. Lapertot, and D. Jaccard. High-Pressure Study of the Ground- and Superconducting-State Properties of CeAu_2Si_2 . *J. Phys. Soc. Jpn.* **86**, 064710 (2017).
- [52] G. W. Scheerer, Z. Ren, G. Lapertot, G. Garbarino, D. Jaccard. Heavy-fermion superconductivity in CeAg_2Si_2 – Interplay of spin and valence fluctuations. *Physica B* **536**, 150-154 (2018).
- [53] G. Knebel, D. Aoki, J.-P. Brison, and J. Flouquet. The Quantum Critical Point in CeRhIn_5 : A Resistivity Study. *J. Phys. Soc. Jpn.* **77**, 114704 (2008).
- [54] F. M. Grosche *et al.* Superconductivity on the threshold of magnetism in CePd_2Si_2 and CeIn_3 . *J. Phys.: Condens. Matter* **13**, 2845-2860 (2001).
- [55] I. Sheikin *et al.* Superconductivity, Upper Critical Field and Anomalous Normal State in CePd_2Si_2 Near the Quantum Critical Point. *J. Low Temp. Phys.* **122**, 591-604 (2001).

- [56] S. Raymond and D. Jaccard. Electronic properties of CePd₂Si₂ under pressure. *Phys. Rev. B* **61**, 8679-8682 (2000).
- [57] H. v. Löhneysen. Fermi-liquid instability at magnetic/nonmagnetic quantum phase transitions. *J. Magn. Magn. Mater.* **200**, 532-551 (1999).
- [58] E. Lengyel, M. Nicklas, H. S. Jeevan, C. Geibel, and F. Steglich. Pressure Tuning of the Interplay of Magnetism and Superconductivity in CeCu₂Si₂. *Phys. Rev. Lett.* **107**, 057001 (2011).
- [59] O. Stockert *et al.* Magnetically driven superconductivity in CeCu₂Si₂. *Nat. Phys.* **7**, 119-124 (2011).
- [60] S. Kittaka *et al.* Multiband Superconductivity with Unexpected Deficiency of Nodal Quasiparticles in CeCu₂Si₂. *Phys. Rev. Lett.* **112**, 067002 (2014).
- [61] H. Ikeda, M.-T. Suzuki, and R. Arita. Emergent Loop-Nodal s_{\pm} -Wave Superconductivity in CeCu₂Si₂: Similarities to the Iron-Based Superconductors. *Phys. Rev. Lett.* **114**, 147003 (2015).
- [62] S. Kittaka *et al.* Thermodynamic study of gap structure and pair-breaking effect by magnetic field in the heavy-fermion superconductor CeCu₂Si₂. *Phys. Rev. B* **94**, 054514 (2016).
- [63] Yamashita *et al.* Fully gapped superconductivity with no sign change in the prototypical heavy-fermion CeCu₂Si₂. *Science Advances* **3**, e1601667 (2017).
- [64] H. Razafimandimby and P. Fulde. On the theory of superconductivity in Kondo lattice systems. *Z. Phys. B - Condensed Matter* **54**, 111-120 (1984).
- [65] H. Jichu, A. D. S. Nagi, B. Jin, T. Matsuura, and Y. Kuroda. Origins of the attractive interactions for the Cooper pairs in dense Kondo systems. *Phys. Rev. B* **35**, 1692-1699 (1987).
- [66] S. Nakatsuji *et al.* Superconductivity and quantum criticality in the heavy-fermion system beta-YbAlB₄. *Nature Phys.* **4**, 603-607 (2008).
- [67] Y. Matsumoto *et al.* Quantum Criticality Without Tuning in the Mixed Valence Compound beta-YbAlB₄. *Science* **331**, 316-319 (2011).
- [68] S. Watanabe and K. Miyake. Quantum Valence Criticality as an Origin of Unconventional Critical Phenomena. *Phys. Rev. Lett.* **105**, 186403 (2010).
- [69] S. Watanabe and K. Miyake. New quantum criticality revealed under pressure. *Jpn. J. Appl. Phys* **56**, 05FA01 (2017).

- [70] S. E. Sebastian *et al.* Metal-insulator quantum critical point beneath the high T_c superconducting dome. *PNAS* **107**, 6175-6179 (2010).
- [71] B. J. Ramshaw *et al.* Quasiparticle mass enhancement approaching optimal doping in a high- T_c superconductor. *Science* **348**, 317-320 (2015).
- [72] E. Vargoz, D. Jaccard. Superconducting and normal properties of CeCu_2Ge_2 at high pressure. *J. Magn. Magn. Mat.* **177**, 294-295 (1998).
- [73] G. Girit, Z. Ren, P. Pedrazzini, D. Jaccard. High pressure investigation of superconducting signatures in CeCu_2Si_2 : ac-magnetic susceptibility, ac-heat capacity, resistivity and thermopower. *Solid State Commun.* **209-210**, 55-58 (2015).
- [74] B. Bellarbi, A. Benoit, D. Jaccard, J. M. Mignot, H. F. Braun. High-pressure valence instability and T_c maximum in superconducting CeCu_2Si_2 . *Phys. Rev. B* **30**, 1182-1187 (1984).
- [75] H. Wilhelm, S. Raymond, D. Jaccard, O. Stockert, and H. v. Loehneysen. From an antiferromagnet to a heavy-fermion system: CeCu_5Au under pressure. *Science and technology of high pressure*, Proc. of AIRAPT-17, ed. M. H. Manghnani. (Universities Press India, Hyderabad, 2000), p. 697.
- [76] H. Wilhelm, D. Jaccard. Calorimetric and transport investigations of $\text{CePd}_{2+x}\text{Ge}_{2-x}$ ($x = 0$ and 0.02) up to 22 GPa. *Phys. Rev. B* **66**, 064428 (2002).

Supplementary Material for

The Dominant Role of Critical Valence Fluctuations on High T_c Superconductivity in Heavy Fermions

Gernot W. Scheerer*, Zhi Ren, Shinji Watanabe, Gérard Lapertot, Dai Aoki,
Didier Jaccard, Kazumasa Miyake

*correspondence to: gernot.scheerer@unige.ch

This file includes:

Table S1

Figs. S1 to S14

References [72-76] cited in the Supplementary Material only

Supplementary Table S1

compound	$\rho_0(p=0)$ [$\mu\Omega\text{cm}$]	ρ_0 (maximum T_c) [$\mu\Omega\text{cm}$]	T_{cr} [K]	maximum T_c [K]	ρ -data first published	T_{cr} from
CeCu ₂ Si ₂	~ 5	25.5(2.0)	-13(4)	1.84	[42]	Fig. S4
CeCu ₂ Si ₂	0.4	5.7(0.2)	-8(3)	2.33	[8]	[8]
CeCu ₂ Si ₂	see Fig. S5	8.5(0.2)	-3.7(7)	2.44	Fig. S5	Fig. S5
CeCu ₂ Ge ₂	~ 2	26(3)	13.6(6.0)	1.47	[72]	Fig. S6
CeAg ₂ Si ₂	5.5	21(2)	12.7(6.0)	1.25	[52]	[52]
CeAu ₂ Si ₂	1.8	9.8(0.2)	-14(6)	2.33	[18]	[18]
CeAu ₂ Si ₂	2.5	20(2)	-13(6)	1.40	[27]	[27]
CeAu ₂ Si ₂	12	43(1)	-25(8)	0.66	[26]	[26]
CePd ₂ Si ₂	~ 4	1.93(0.05)	-44(12)	0.40*	[56]	Fig. S7
CePd ₂ Si ₂	2.6	1.83(0.05)	-49(15)	0.34*	[56]	Fig. S8
CePd ₂ Si ₂	1.25	1.1(0.05)	-48(12)	0.441	[19]	Fig. S9
CePd ₂ Si ₂	0.6	0.44(0.05)	-55(15)	0.325	[19]	Fig. S10
CeCu ₆	12.4	-- [†]	-17(9)	-- [†]	[34]	Fig. S11
CeCu ₅ Au	28.9	33(0.5)	-6.5(1.5)	0.11**	[75]	Fig. S12
CeRhIn ₅	0.2 ^{T=2 K}	2.8(0.1)	-9(3)	2.26	[17]	[17]
CeRhIn ₅	0.011	1.1(0.05)	-8(3)	2.25	[17]	[17]
CeIrIn ₅	1.7 ^{T=1.5 K}	0.37(0.02)	-28(12)	1	Fig. S13	Fig. S13

Table S1. Experimental values of $\rho_0(p=0)$, ρ_0 taken at the pressure of maximum T_c , T_{cr} , and maximum T_c of several Ce-HF samples. Note that “maximum T_c ” refers to the maximum value of the bulk-superconducting transition temperature as function of pressure in a given sample, except for two CePd₂Si₂* samples and CeCu₅Au**. In general, bulk superconductivity coincides with zero resistivity, in agreement with ac heat capacity or magnetic susceptibility signals [8,18,51,73]. Resistivity ρ was measured in the basal plane or along the a-axis of the tetragonal structure, except for CeCu₆ and CeCu₅Au, where ρ was investigated for the b-axis of the orthorhombic structure. * T_c from resistivity transition offset criterion, where ρ does not completely drop to zero [56]. ** T_c from resistivity transition onset criterion [75]. [†] By matching the (p - T) phase diagrams of CeCu₆ and CeCu₅Au, hypothetical SC in CeCu₆ corresponds to negative pressure $p \approx -0.5$ GPa.

Supplementary Figure S1

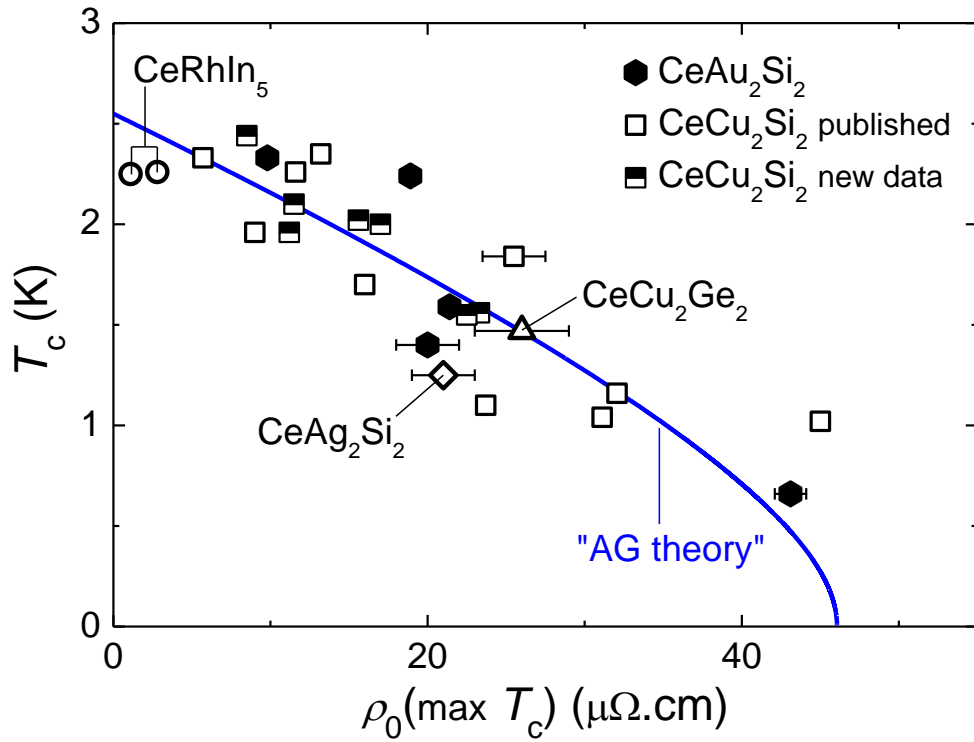


Fig. S1. Superconducting T_c vs. residual resistivity ρ_0 of the CeCu_2Si_2 -family and CeRhIn_5 (ρ_0 taken at the pressure of maximum T_c). All data points are from independent pressure experiments done in Geneva. Data for CeRhIn_5 from [17], CeCu_2Ge_2 from [72], and CeAg_2Si_2 from [52]. Filled hexagons refer to published data of CeAu_2Si_2 [18,26,27,51]. Empty cubes refer to published data of CeCu_2Si_2 [7,8,36,42,44,73,74]. Half-filled cubes refer to new data of CeCu_2Si_2 .

Supplementary Figure S2

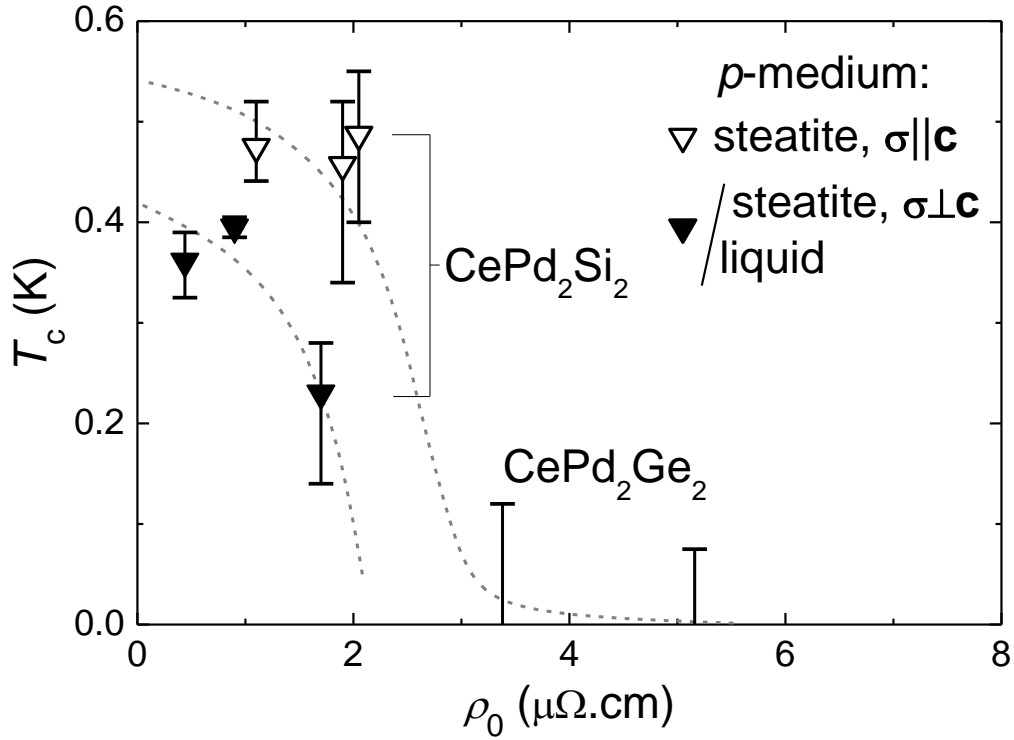


Fig. S2. Superconducting T_c vs. residual resistivity ρ_0 of CePd_2Si_2 [19,43,55,56] and CePd_2Ge_2 [76] (ρ_0 taken at the pressure of maximal T_c). Triangle symbols indicate the T_c defined at the 50% drop of ρ . The onset and end of the resistive superconducting transition are indicated by vertical bars. The dashed lines are guides to the eyes. An enhanced T_c due to strain effects [19] is observed in soft-solid steatite pressure medium with $\sigma \parallel \mathbf{c}$ compared to liquid pressure medium or steatite with $\sigma \perp \mathbf{c}$, and two data sets with qualitatively similar behavior can be distinguished.

Supplementary Figure S3

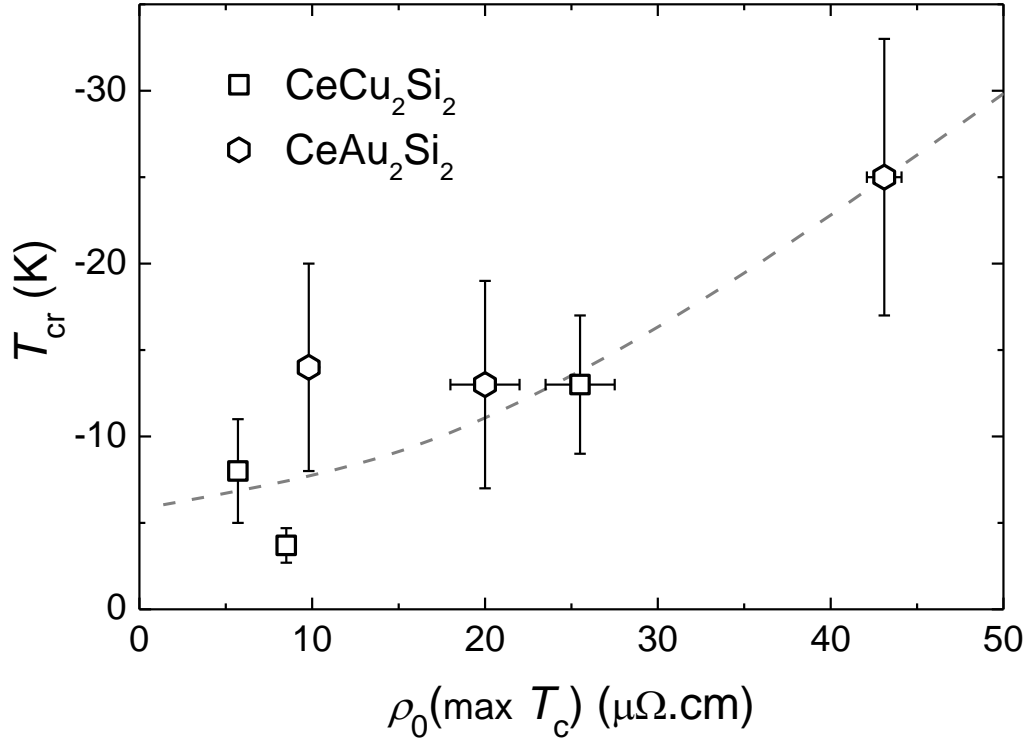


Fig. S3. Critical temperature T_{cr} vs. residual resistivity ρ_0 of CeCu_2Si_2 and CeAu_2Si_2 (ρ_0 taken at the pressure of maximal T_c). As qualitatively predicted by CVF theory [23], the two parameters ρ_0 and T_{cr} are correlated. Disorder induces an additional smearing of the VCO-induced resistivity collapse resulting in reduced experimental T_{cr} value.

Supplementary Figure S4

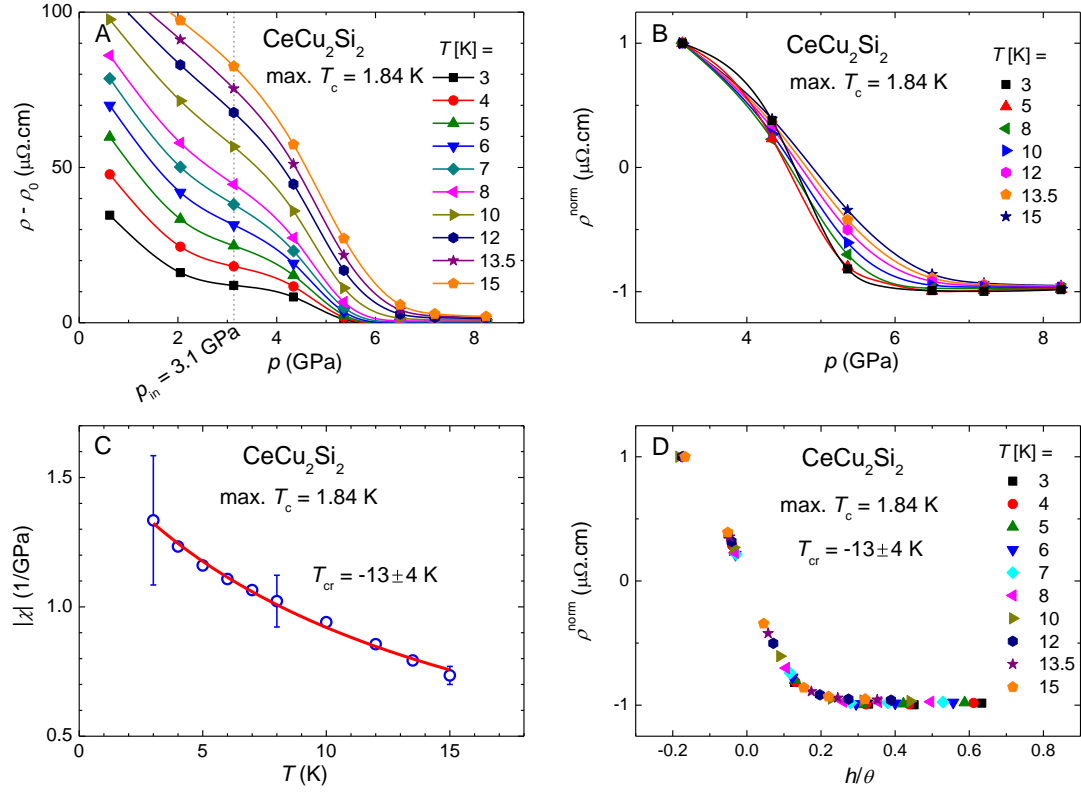


Fig. S4. Resistivity scaling analysis of a CeCu₂Si₂ sample with $T_c = 1.84$ K. $\rho(T)$ -data first published in [42]. (A) Resistivity isotherms $\rho^* = \rho - \rho_0$ vs. pressure p at temperatures T from 3 up to 15 K. (B) Normalized resistivity ρ^{norm} vs. p . (C) Slope $\chi = (d\rho^{\text{norm}}/dp)_{p_{\text{VCO}}}$ vs. T . The red line represents a fit to the data with $\chi \sim 1/(T - T_{\text{cr}})$. The fit gives $T_{\text{cr}} = -13 \pm 4$ K. Error bars on χ are shown for representative data points. (D) Normalized resistivity ρ^{norm} vs. the generalized distance h/θ .

Supplementary Figure S5

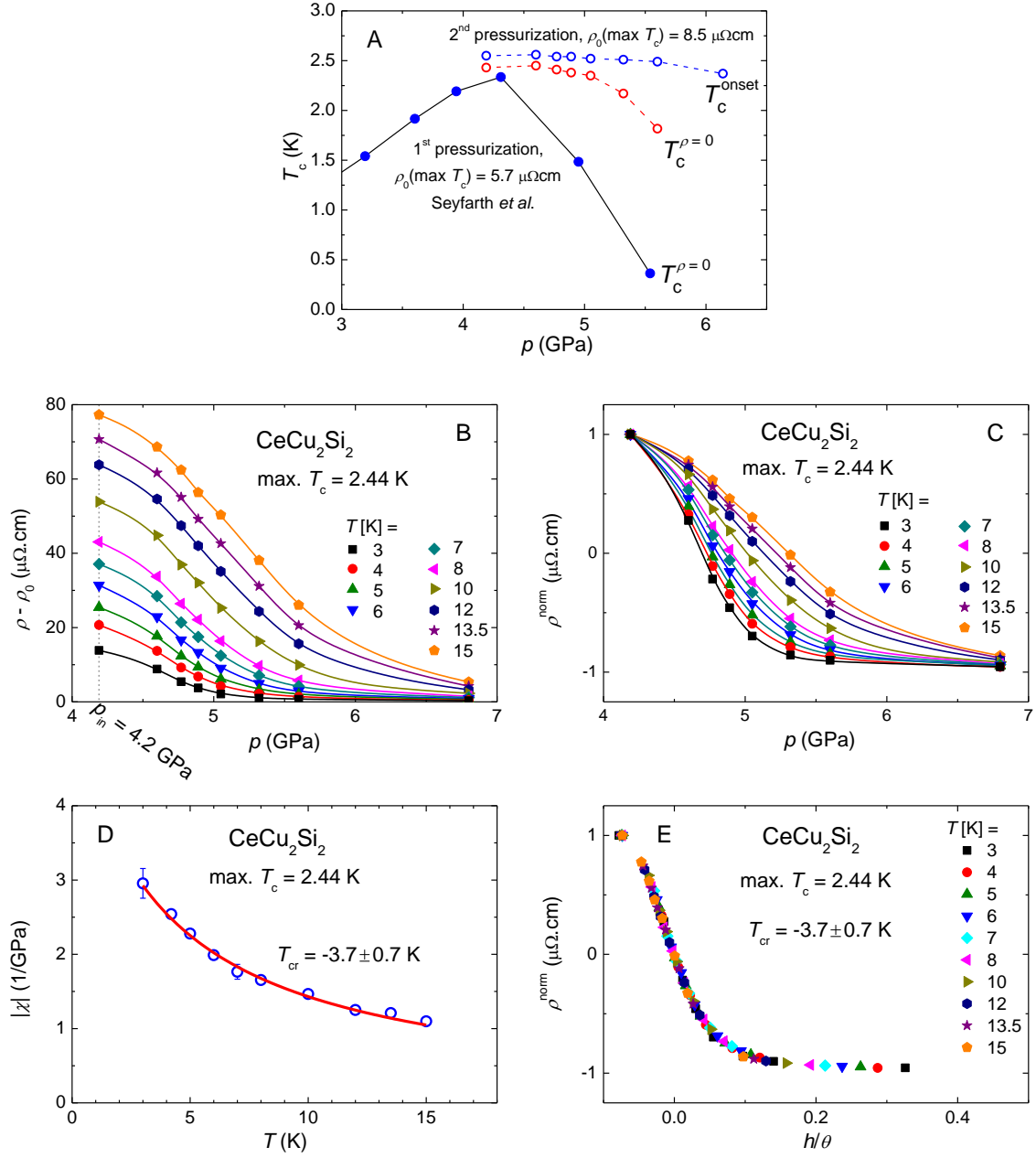


Fig. S5. Resistivity scaling analysis of a CeCu_2Si_2 sample with $T_c = 2.44$ K (record value!). Unpublished data of the second pressure cycle of Seyfarth *et al.* [8]. After a partial depressurization down to about 4 GPa, pressure was increased again by small steps for a better investigation of the VCO. (A) T_c vs. pressure of the first and second pressure cycles. Interestingly, the maximal T_c of the second cycle was a bit higher and the SC dome shifted up by about 0.5 GPa associated to a 50% increase in ρ_0 . (B) Resistivity isotherms $\rho^* = \rho - \rho_0$ vs. pressure p at temperatures T from 3 up to 15 K. (C) Normalized resistivity ρ^{norm} vs. p . (D) Slope $\chi = (d\rho^{\text{norm}}/dp)_{p\text{VCO}}$ vs. T . The red line represents a fit to the data with $\chi \sim 1/(T - T_{\text{cr}})$. The fit gives $T_{\text{cr}} = -3.7 \pm 0.7$ K. Error bars on χ are shown for representative data points. (E) Normalized resistivity ρ^{norm} vs. the generalized distance h/θ . With a high pressure-run density in the VCO regime, these data give the most accurate T_{cr} value.

Supplementary Figure S6

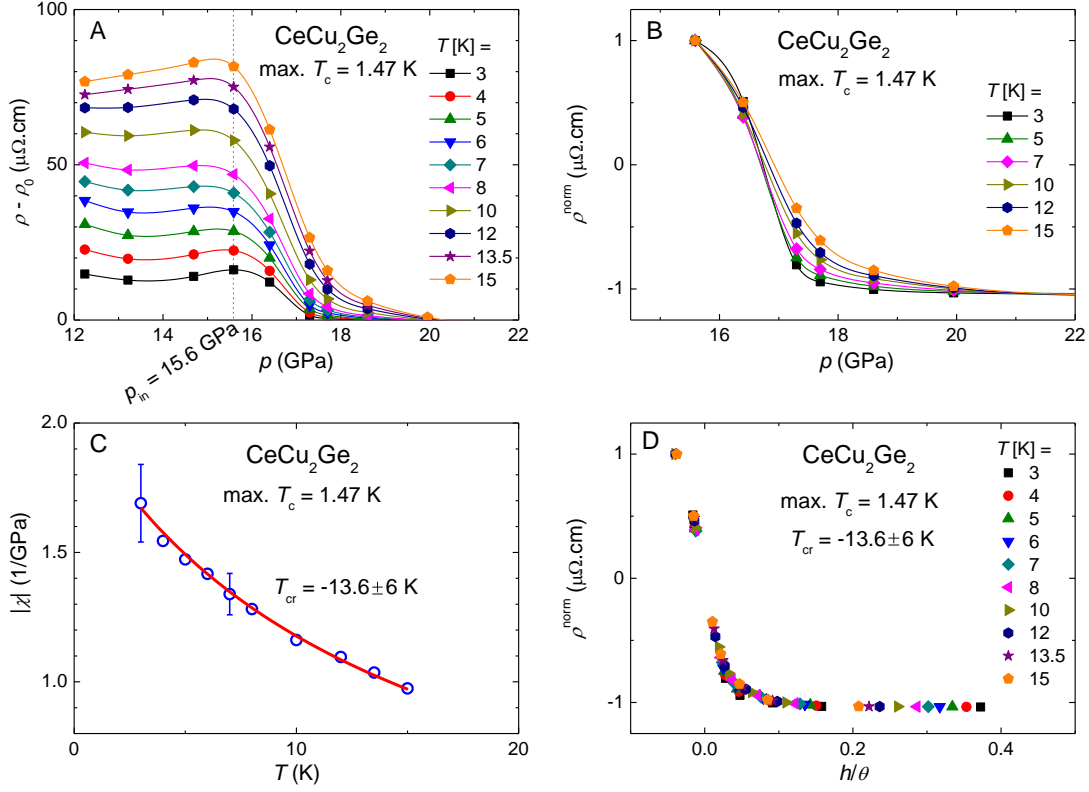


Fig. S6. Resistivity scaling analysis of a CeCu₂Ge₂ sample with $T_c = 1.47$ K. $\rho(T)$ -data first published in [72]. (A) Resistivity isotherms $\rho^* = \rho - \rho_0$ vs. pressure p at temperatures T from 3 up to 15 K. (B) Normalized resistivity ρ^{norm} vs p . (C) Slope $\chi = (d\rho^{\text{norm}}/dp)_{p_{\text{VCO}}}$ vs. T . The red line represents a fit to the data with $\chi \sim 1/(T - T_{\text{cr}})$. The fit gives $T_{\text{cr}} = -13.6 \pm 6$ K. Error bars on χ are shown for representative data points. (D) Normalized resistivity ρ^{norm} vs. the generalized distance h/θ .

Comment on scaling analysis of CePd₂Si₂:

From the “raw” resistivity isotherms ρ^* (obtained in steatite p -medium) it is obvious that the resistivity collapse is slower than in the other compounds (see main text Fig. 2). Thus, the CEP should be at more negative temperature, which would imply a slower change of the slope χ as a function of T , and a bigger error on T_{cr} extracted by fitting with $\chi \sim 1/(T - T_{\text{cr}})$. Fortunately in CePd₂Si₂, the relatively high value $T_1^{\text{max}} \sim 100$ K at the pressure of the VCO allows to extend the analysis to higher temperature. By fitting $\chi(T)$ over an extended T -scale, the error of T_{cr} is reduced. Very robust scaling analysis is obtained for four CePd₂Si₂ samples (see Figs. S7-S10).

With a CEP at very negative temperature in CePd₂Si₂, the decrease of ρ^* is extended over a larger pressure scale compared to e.g. CeCu₂Si₂. For $T > T_N$, the decrease of ρ^* sets in already at pressures well below p_c . We have chosen p_{in} with the condition $p_{\text{in}} > p_c$ to go as low as possible in temperature to get the closest to the CEP. We have verified that the conditions $p_{\text{in}} < p_c$ and $T > T_N$ give similar results, with T_{cr} values within the error bar.

Supplementary Figure S7

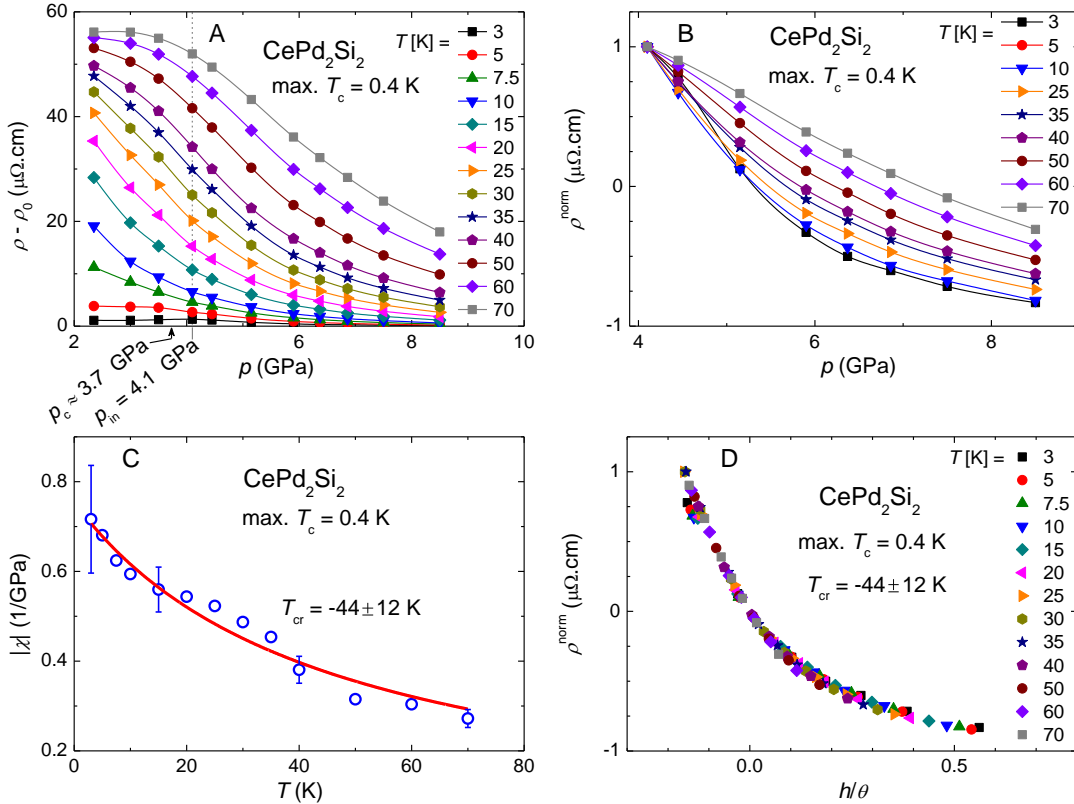


Fig. S7. Resistivity scaling analysis of a CePd₂Si₂ sample with $T_c = 0.4$ K. $\rho(T)$ -data first published in [56]. (A) Resistivity isotherms $\rho^* = \rho - \rho_0$ vs. pressure p at temperatures T from 3 up to 70 K. (B) Normalized resistivity ρ^{norm} vs. p . (C) Slope $\chi = (d\rho^{\text{norm}}/dp)_{p\text{VCO}}$ vs. T . The red line represents a fit to the data with $\chi \sim 1/(T - T_{\text{cr}})$. The fit gives $T_{\text{cr}} = -44 \pm 12$ K. Error bars on χ are shown for representative data points. (D) Normalized resistivity ρ^{norm} vs. the generalized distance h/θ .

Supplementary Figure S8

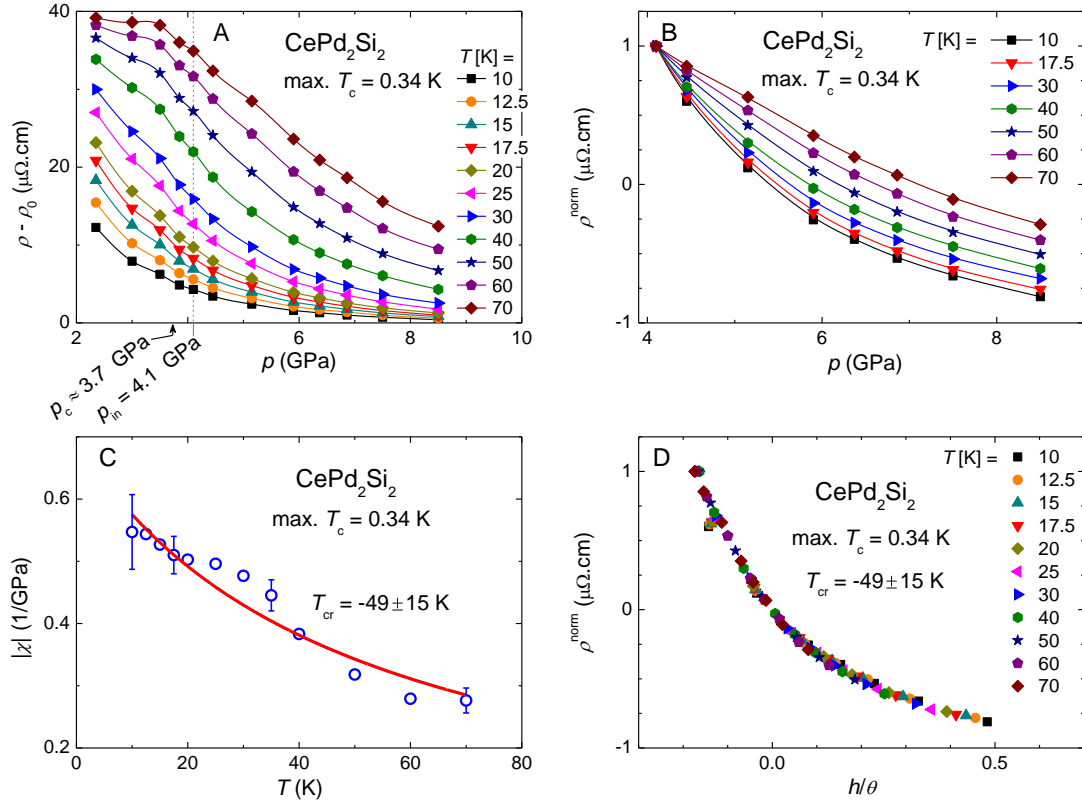


Fig. S8. Resistivity scaling analysis of a CePd_2Si_2 sample with $T_c = 0.34$ K. $\rho(T)$ -data first published in [56]. (A) Resistivity isotherms $\rho^* = \rho - \rho_0$ vs. pressure p at temperatures T from 10 up to 70 K. (B) Normalized resistivity ρ^{norm} vs. p . (C) Slope $\chi = (d\rho^{\text{norm}}/dp)_{p_{\text{VCO}}}$ vs. T . The red line represents a fit to the data with $\chi \sim 1/(T - T_{cr})$. The fit gives $T_{cr} = -49 \pm 15$ K. Error bars on χ are shown for representative data points. (D) Normalized resistivity ρ^{norm} vs. the generalized distance h/θ .

Supplementary Figure S9

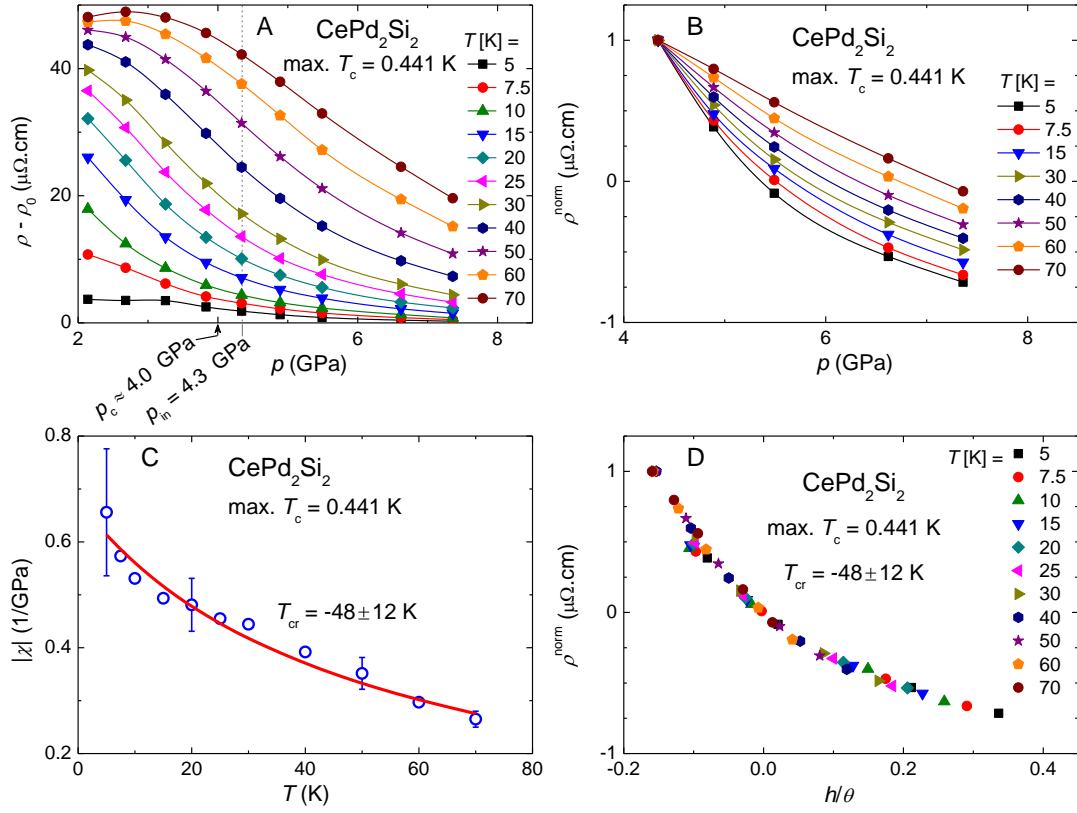


Fig. S9. Resistivity scaling analysis of a CePd₂Si₂ sample with $T_c = 0.441$ K. $\rho(T)$ -data first published in [19]. (A) Resistivity isotherms $\rho^* = \rho - \rho_0$ vs. pressure p at temperatures T from 5 up to 70 K. (B) Normalized resistivity ρ^{norm} vs. p . (C) Slope $\chi = (d\rho^{\text{norm}}/dp)_{p_{\text{VCO}}}$ vs. T . The red line represents a fit to the data with $\chi \sim 1/(T - T_{\text{cr}})$. The fit gives $T_{\text{cr}} = -48 \pm 12$ K. Error bars on χ are shown for representative data points. (D) Normalized resistivity ρ^{norm} vs. the generalized distance h/θ .

Supplementary Figure S10

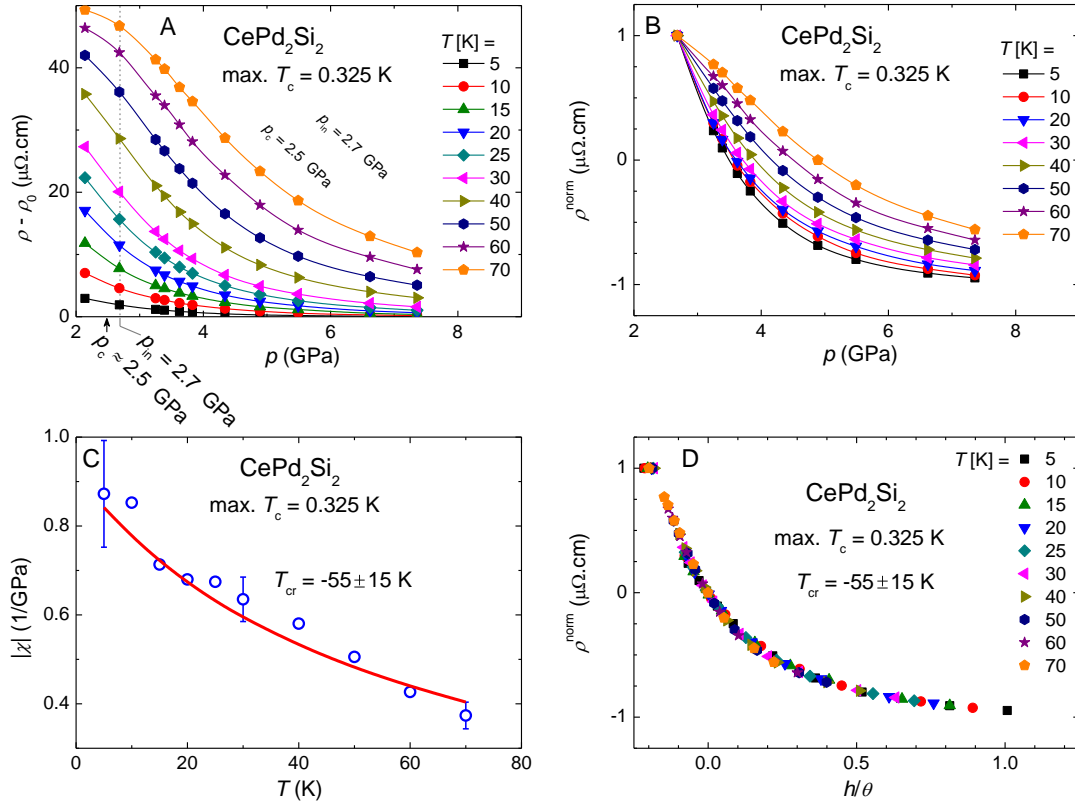


Fig. S10. Resistivity scaling analysis of a CePd₂Si₂ sample with $T_c = 0.325$ K. $\rho(T)$ -data first published in [19]. (A) Resistivity isotherms $\rho^* = \rho - \rho_0$ vs. pressure p at temperatures T from 5 up to 70 K. (B) Normalized resistivity ρ^{norm} vs. p . (C) Slope $\chi = (d\rho^{\text{norm}}/dp)_{p_{\text{VCO}}}$ vs. T . The red line represents a fit to the data with $\chi \sim 1/(T - T_{\text{cr}})$. The fit gives $T_{\text{cr}} = -55 \pm 15$ K. Error bars on χ are shown for representative data points. (D) Normalized resistivity ρ^{norm} vs. the generalized distance h/θ .

Supplementary Figure S11

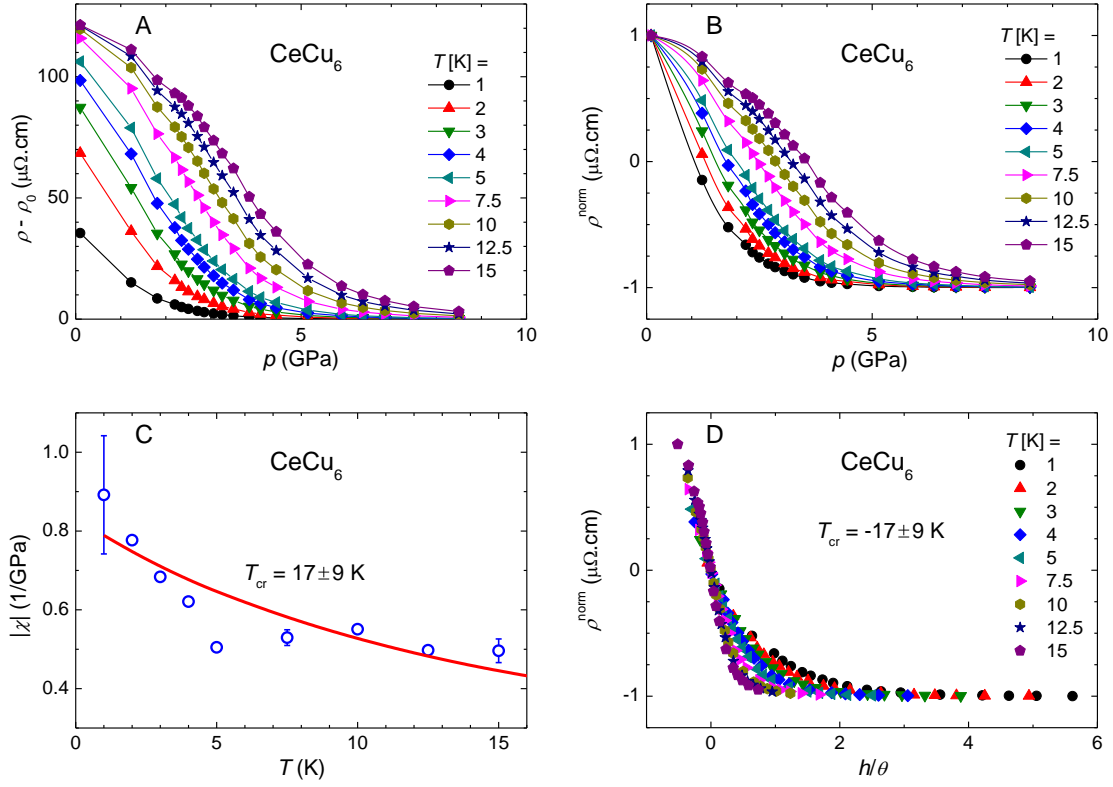


Fig. S11. Resistivity scaling analysis of a CeCu₆ sample. $\rho(T)$ -data obtained in steatite p -medium first published in [34]. (A) Resistivity isotherms $\rho^* = \rho - \rho_0$ vs. pressure p at temperatures T from 1 to 15 K. Looking on the “raw” resistivity data ρ^* , we suspect that measurement errors for pressures up to 2 GPa are most likely due to the combined effect of error on p and bad thermalization of the sample (fast cooldown). (B) Normalized resistivity ρ^{norm} vs p . (C) Slope $\chi = (d\rho^{\text{norm}}/dp)_{p_{\text{VCO}}}$ vs. T . The red line represents a fit to the data with $\chi \sim 1/(T - T_{\text{cr}})$. The fit gives $T_{\text{cr}} = -17 \pm 9$ K. Error bars on χ are shown for representative data points. The bad overlap of fit and data is presumably due to the measurement errors noted before. Also, a low pressure-run density at the beginning of the pressurization results in a high error on χ . (D) Normalized resistivity ρ^{norm} vs. the generalized distance h/θ . The curves do not collapse on a single scaling function. For now, it is not clear if this is intrinsic to CeCu₆ or due to the measurement errors only. A change of regime ascribed to the crystal field effect [34] may interfere.

Supplementary Figure S12

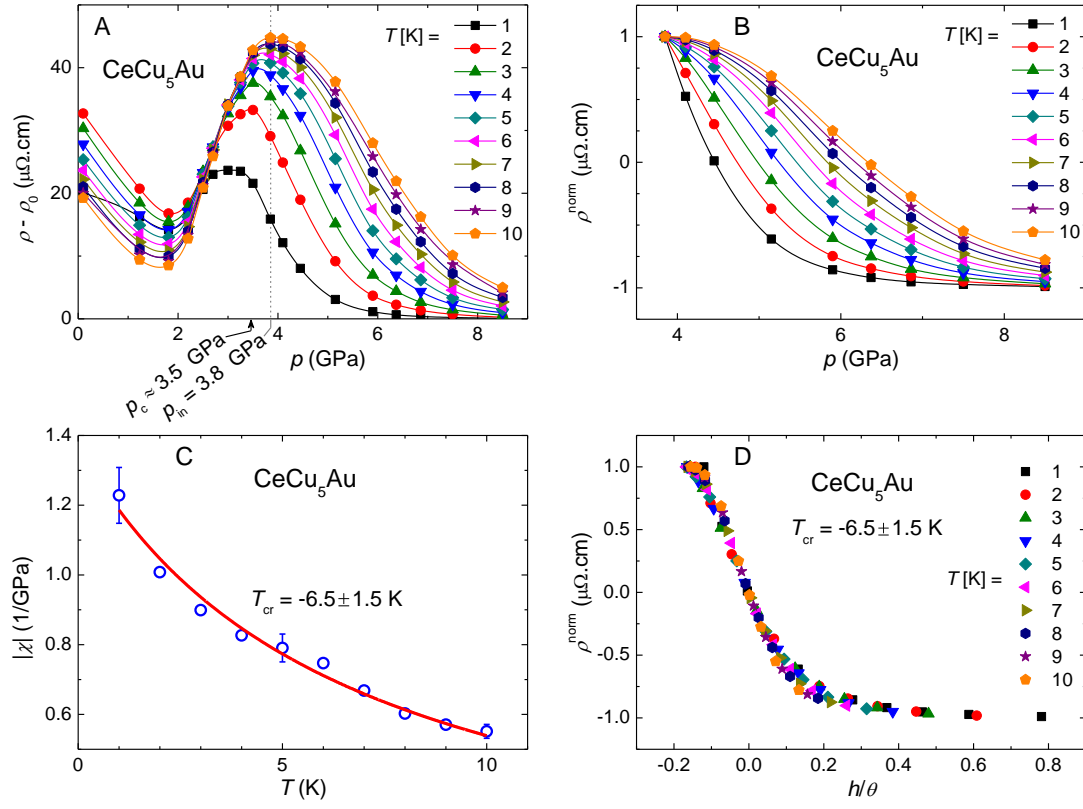


Fig. S12. Resistivity scaling analysis of a CeCu₅Au sample. $\rho(T)$ -data first published in [75]. (A) Resistivity isotherms $\rho^* = \rho - \rho_0$ vs. pressure p at temperatures T from 1 up to 10 K. Note that the scaling analysis is limited to $T \leq 10$ K because of a low $T_1^{\text{max}} \sim 25$ K at the VCO. (B) Normalized resistivity ρ^{norm} vs. p . (C) Slope $\chi = (d\rho^{\text{norm}}/dp)_{p\text{VCO}}$ vs. T . The red line represents a fit to the data with $\chi \sim 1/(T - T_{\text{cr}})$. The fit gives $T_{\text{cr}} = -6.5 \pm 1.5$ K. Error bars on χ are shown for representative data points. (D) Normalized resistivity ρ^{norm} vs. the generalized distance h/θ .

Supplementary Figure S13

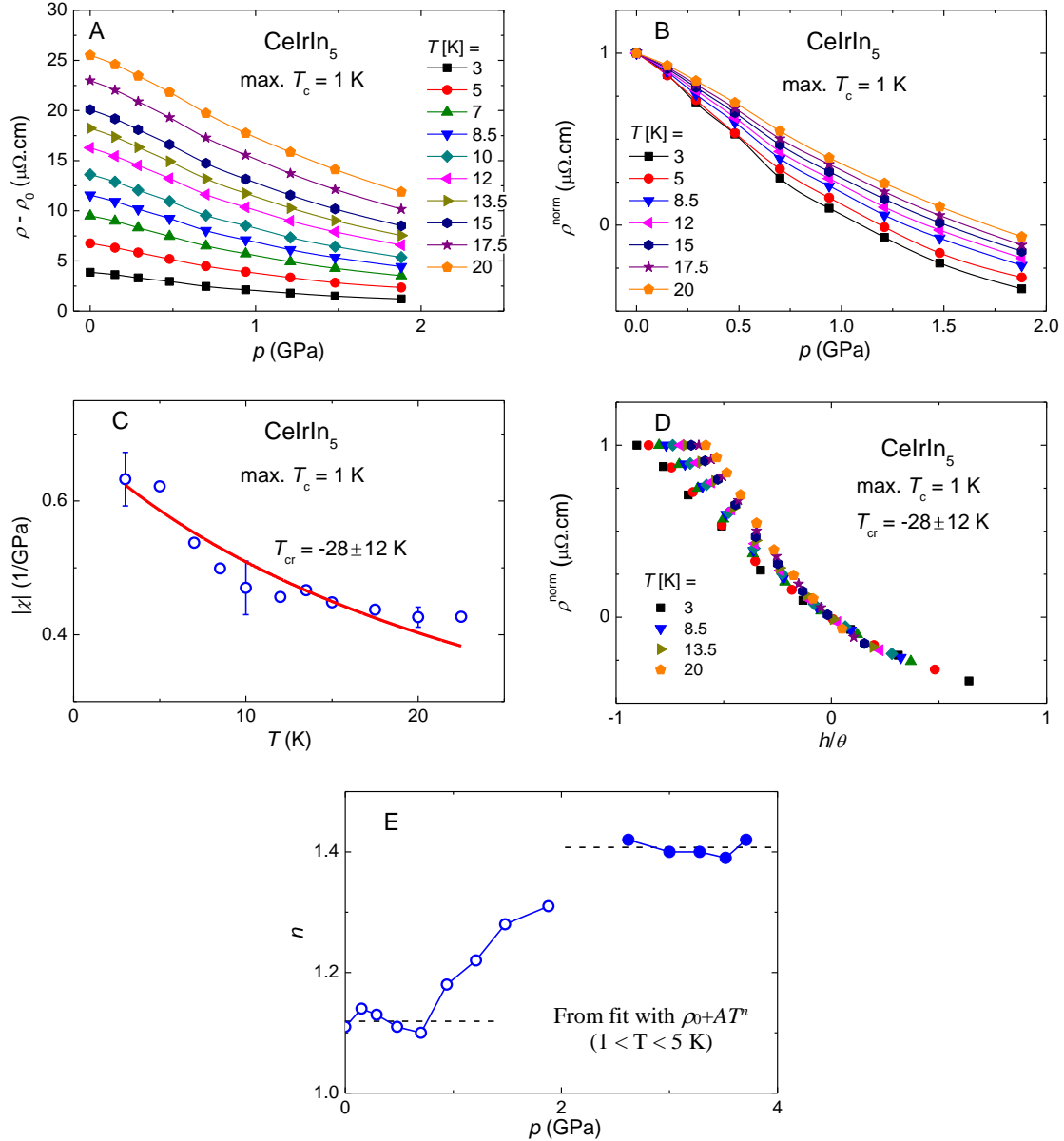


Fig. S13. Resistivity scaling analysis of a CeIrIn₅ sample. (A) Resistivity isotherms $\rho^* = \rho - \rho_0$ vs. pressure p at temperatures T from 3 up to 20 K. (B) Normalized resistivity ρ^{norm} vs. p . (C) Slope $\chi = (d\rho^{\text{norm}}/dp)_{p_{\text{VCO}}}$ vs. T . The red line represents a fit to the data with $\chi \sim 1/(T - T_{\text{cr}})$. The fit gives $T_{\text{cr}} = -28 \pm 12$ K. Error bars on χ are shown for representative data points. (D) Normalized resistivity ρ^{norm} vs. the generalized distance h/θ . The ρ^* isotherms collapse on a single curve only for $h/\theta > 0$. (E) Exponent n versus pressure p , obtained by fitting low-temperature resistivity $\rho(T)$ with $\rho_0 + AT^n$. Open symbols: data corresponding to Fig. S13A, full symbols: preliminary data from a new high-pressure experiment. The behavior of $n(p)$ hints to a pressure-induced change of regime, which may explain why the isotherms do not collapse for $h/\theta < 0$.

Supplementary Figure S14

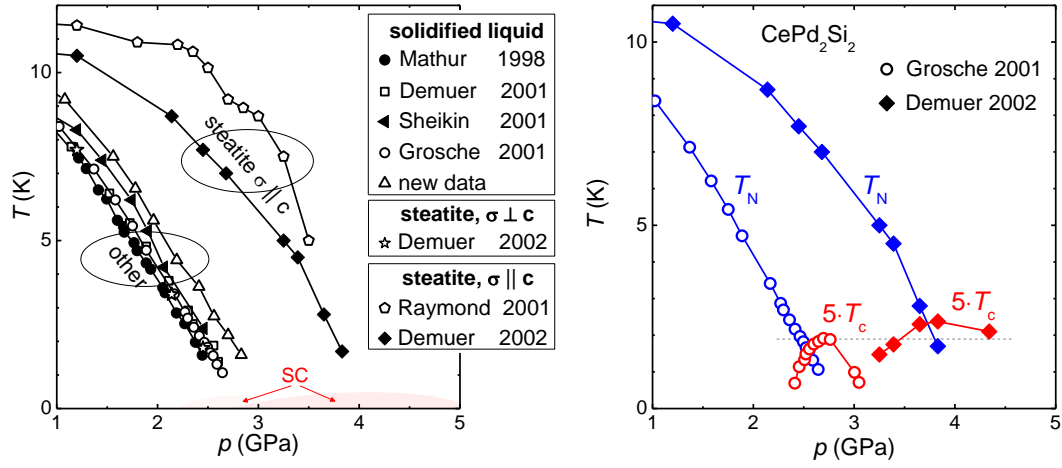


Fig. S14. Pressure-temperature phase diagram of CePd_2Si_2 samples measured in “solidified-liquid” [3,43,54,55] and “soft-solid-steatite” [19,56] pressure-transmitting medium (“solidified-liquid” = He, pentane, Daphne oil). Left-panel: all known data of the T_N transition line. A linear decrease of T_N occurs in “solidified-liquid” or steatite with stress $\sigma \perp c$. A more rapid vanishing of T_N occurs in steatite with stress $\sigma \parallel c$. The corresponding superconducting phases are represented schematically. Right panel: Phase diagram of two samples of similar quality as indicated by their residual resistivity $\rho_0 \approx 1.1 \mu\Omega\text{cm}$. A steeper collapse of the antiferromagnetic transition temperature T_N seems to favor higher superconducting T_c . Noteworthy, Demuer *et al.* [19] have observed a strain-driven enhancement of T_c . Two samples have been measured simultaneously in steatite with $\sigma \perp c$ and $\sigma \parallel c$, respectively. Despite lower sample quality, a higher T_c was found for $\sigma \parallel c$.

References

- [72] E. Vargoz, D. Jaccard, J. Magn. Magn. Mat. **177**, 294-295 (1998).
- [73] G. Giriat, Z. Ren, P. Pedrizzini, D. Jaccard, Solid State Commun. **209-210**, 55-58 (2015).
- [74] B. Bellarbi, A. Benoit, D. Jaccard, J. M. Mignot, H. F. Braun, Phys. Rev. B **30**, 1182-1187 (1984).
- [75] H. Wilhelm, S. Raymond, D. Jaccard, O. Stockert, and H. v. Loehneysen, *Science and technology of high pressure*, Proc. of AIRAPT-17, ed. M. H. Manghnani. (Universities Press India, Hyderabad, 2000), p. 697.
- [76] H. Wilhelm, D. Jaccard, Phys. Rev. B **66**, 064428 (2002).